Distribution of active rock uplift along the eastern margin of the Tibetan Plateau: Inferences from bedrock channel longitudinal profiles

Eric Kirby[1] and Kelin X. Whipple

Department of Earth, Atmospheric, and Planetary Sciences, Massachusetts Institute of Technology, Cambridge, Massachusetts, USA

Wenqing Tang and Zhiliang Chen

Chengdu Institute of Geology and Mineral Resources, Chengdu, Sichuan, China

Received 31 July 2001; revised 9 October 2002; accepted 18 November 2002; published 26 April 2003.

[1] Current models of long-term river incision into bedrock suggest that the local rate of differential rock uplift should exert a primary control on the gradient of channel longitudinal profiles. However, discrimination of this effect from the influence of variations in substrate erodibility, sediment flux, precipitation, and transient changes in profile shape has proved difficult in practice. Here we investigate the controls on the spatial distribution of bedrock channel gradients adjacent to the Sichuan Basin in an effort to assess the degree and nature of active deformation along this margin of the Tibetan Plateau. Analysis of river longitudinal profiles utilizing a channel steepness index (a measure of profile gradient normalized for drainage area) reveals a zone of anomalously steep channels adjacent to the topographic front of the plateau margin. Channel profiles are systematically less steep in their headwater reaches on the plateau and in their lower reaches east of the plateau margin. Comparison of steepness indices to mapped lithologic variations reveals that lithology has only a limited influence on channel gradient in this field area. We observe no systematic relationship between steepness indices and upstream drainage area; channels of all size are steeper near the plateau margin. We argue that these systematic changes are not readily explained as a consequence of increased sediment flux or of orographic precipitation. We are led to conclude that steep channel profiles along the topographic front of the plateau reflect active differential rock uplift between this region and the foreland. *INDEX TERMS:* 1824 Hydrology: Geomorphology (1625); 8107 Tectonophysics: Continental neotectonics; 8102 Tectonophysics: Continental contractional orogenic belts; *KEYWORDS:* bedrock rivers, neotectonics, fluvial geomorphology, Tibetan Plateau, Sichuan Basin, East Tibet

Citation: Kirby, E., K. X. Whipple, W. Tang, and Z. Chen, Distribution of active rock uplift along the eastern margin of the Tibetan Plateau: Inferences from bedrock channel longitudinal profiles, *J. Geophys. Res.*, *108*(B4), 2217, doi:10.1029/2001JB000861, 2003.

1. Motivation

[2] The recognition that mass redistribution by erosion represents a governing force in the tectonic evolution of orogenic systems [*Beaumont et al.*, 1992; *Molnar and England*, 1990] spurred a decade of intensive research into the interrelationships between tectonic and surface processes. One of the primary outgrowths of this work is the understanding that much of the tempo and style of landscape evolution in active mountain belts is dictated by the processes of river incision into bedrock [e.g., *Seidl and Dietrich*, 1992; *Tinkler and Wohl*, 1998]. The bedrock channel network dictates critical relationships among relief, elevation, and denudation rate [*Howard*, 1994; *Howard et al.*, 1994; *Whipple et al.*, 1999] and conveys signals of tectonic and climatic change across landscapes, effectively setting landscape response time [*Whipple and Tucker*, 1999]. The rate of channel incision sets the lower boundary condition for hillslopes and thus fundamentally influences denudation rates across the landscape.

[3] Current models of bedrock channel incision in tectonically active regions consider that channel gradients are set by a competition between the local rate of differential rock uplift (relative to a fixed, external base level) and channel incision rate [*Howard*, 1994]. Consequently, analysis of channel gradients and longitudinal profiles provides a promising means of exploring the spatial distribution of rock uplift in an actively deforming orogen [e.g., *Hack*,

[1]Now at Department of Geosciences, Pennsylvania State University, University Park, Pennsylvania, USA.

0148-0227/03/2001JB000861$09.00

1957, 1973; *Kirby and Whipple*, 2001; *Snyder et al.*, 2000], provided one can account for the influence of lithologic variations, sediment flux, nonuniform distributions of precipitation, and transient profile evolution. In a pioneering analysis of transverse rivers crossing the Himalaya, *Seeber and Gornitz* [1983] argued that anomalously high channel gradients in the Higher Himalaya likely reflected rock uplift localized beneath the range crest, a prediction borne out, at least in the short-term, by recent geodetic and leveling surveys [*Bilham et al.*, 1997; *Jackson and Bilham*, 1994].

[4] In this paper we analyze downstream changes in channel profile gradient of rivers draining the eastern margin of the Tibetan Plateau in an effort to extract information about the spatial distribution of active rock uplift along this margin. Our efforts are motivated in large part by competing hypotheses for the evolution of the margin. The region has long been considered a locus of active shortening between the plateau and its foreland [e.g., *Avouac and Tapponnier*, 1993]. However, recent geodetic [*Chen et al.*, 2000; *King et al.*, 1997] and geologic [*Burchfiel et al.*, 1995] investigations indicate that there is little resolvable shortening across this margin. *Royden et al.* [1997] proposed that much of the topography in eastern Tibet developed as a consequence of thickening by flow of the lower crust with little attendant disruption of surface features. This model predicts, in a general way, that rock uplift may be decoupled from upper crustal shortening. Consequently, analysis of channel profiles may provide a means of identifying spatial gradients in rock uplift rate across this margin and thus place important constraints on dynamic models for the evolution of this region of the plateau.

2. Background: Active Tectonics in Eastern Tibet

[5] The eastern margin of the Tibetan Plateau adjacent to the Sichuan Basin is one of the world's great continental escarpments. Elevations rise from ~500 m in the Sichuan Basin to peak elevations exceeding 6500 m over a distance of 40–60 km. Mean elevations on the plateau to the west range from 3500 to 4000 m (Figure 1). For ~200 km north of the Sichuan Basin, the topographic margin of the plateau trends north-south and coincides with a high mountain range, the Min Shan. Peak elevations in the range are ~5500 m and stand approximately 2 km above the plateau to the west and some 4 km above the highlands of the West Qinling mountains to the east. North of ~34°N, the margin of the plateau ceases to be a readily discernable feature, and plateau elevations grade gently into regional elevations ~1000 m [*Clark and Royden*, 2000].

[6] Despite the topography along this margin of the plateau, recent space geodetic surveys indicate that active shortening between the plateau and its foreland is less than 2–3 mm/yr and is within uncertainty of zero [*Chen et al.*, 2000; *King et al.*, 1997]. Furthermore, although the region was subject to severe upper crustal shortening during the Mesozoic, very little shortening appears to have taken place during Cenozoic time [*Burchfiel et al.*, 1995]. Indeed, Cenozoic terrestrial sediments in the Sichuan Basin are restricted to a thin (< 700 m) veneer in the southwestern corner of the basin [*Burchfiel et al.*, 1995] and indicate that the basin underwent little flexural subsidence during development of the plateau [*Royden et al.*, 1997]. These observations led *Royden et al.* [1997] to suggest that plateau development and subsequent evolution were driven by thickening in a weak lower crust that was rheologically decoupled from upper crustal deformation. This model predicts that the isostatic and dynamic response to such thickening should result in differential rock uplift across the margin of the plateau.

[7] Geologic evidence for recent deformation exists in the Min Shan region north of the Sichuan Basin (Figure 1). Here, west directed tilting recorded by remnant Quaternary basins along the western flank of the range suggests that fairly rapid differential rock uplift is occurring between the range crest and the Tibetan Plateau [*Kirby et al.*, 2000]. However, along the margin of the Sichuan Basin southeast of the range (Figure 1), frontal thrust faults are overlapped by Early Jurassic terrestrial sediments [*Burchfiel et al.*, 1995] that restrict the timing of the most recent displacement on these structures to the Mesozoic. There are a series of discontinuous faults along the eastern flank of the Min Shan (Figure 1) [*Chen et al.*, 1994b; *Kirby et al.*, 2000], but their relationship to the high topography of the range is ambiguous [*Kirby et al.*, 2000]. Thus stream profiles in this region may provide important insight into the extent to which active rock uplift in the Min Shan extends into the foreland to the east and southeast of the plateau margin.

[8] To the south of the Min Shan, the absence of Quaternary sediments prevents ready evaluation of deformation along the margin of the Sichuan Basin. However, there are several regionally extensive fault zones that are suspected of having some degree of Quaternary activity [*Burchfiel et al.*, 1995]. These include a series of frontal faults along the margin of the Sichuan Basin, collectively here termed the Guan Xian-An Xian fault system, a system of thrust faults that carry basement massifs in their hanging walls, termed the Yingxiu-Beichuan fault system [*Chen et al.*, 1994a; *Chen and Wilson*, 1996], and the Wenchuan-Maowen fault zone [*Burchfiel et al.*, 1995; *Chen and Wilson*, 1996] (Figure 1). The nature and significance of recent activity on these structures is debated [cf. *Burchfiel et al.*, 1995; *Chen et al.*, 1994b]. Consequently, stream profiles may provide an indication as to the degree of activity on these structures and allow us to assess their potential role in accommodating active deformation along this margin.

3. Approach and Scope

[9] This paper develops a method for examining systematic changes in channel gradient across a landscape within the context of the detachment-limited unit stream power incision model [*Howard et al.*, 1994]. Our approach builds upon recent theoretical considerations of the dynamics of the stream power incision model [*Whipple and Tucker*, 1999], empirical evaluation of steady state channel profiles under conditions of uniform lithology and uplift rate [*Snyder et al.*, 2000], and analysis of channel response to spatial gradients in rock uplift rate [*Kirby and Whipple*, 2001]. Essentially, we utilize a generalized version of the stream gradient index [*Hack*, 1973] to explore the spatial variability of channel gradient. Although we do not explicitly consider the role of sediment flux in the analysis, we recognize its potential influence [e.g., *Sklar and Dietrich*, 1998] and qualitatively consider it in our interpretation.

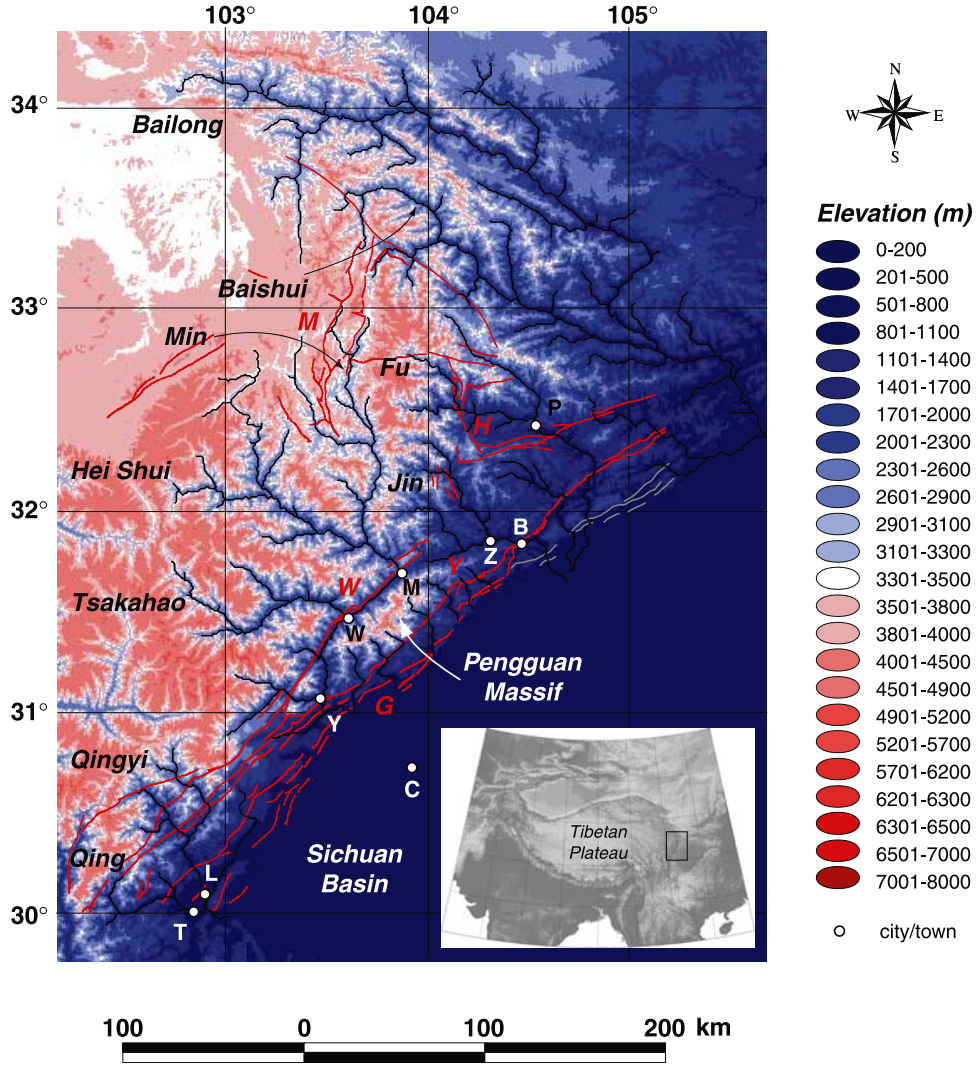

Figure 1. Topography of the eastern margin of the Tibetan Plateau adjacent to and north of the Sichuan Basin (inset shows location). Major river basins draining the region are shown in black. Major faults are shown in red (W, Wenchuan-Maowen fault zone; G, Guanxian-Anxian fault zone; H, Huya fault; M, Min Jiang fault zone; Y, Yingxiuwan-Beichuan fault system), while those in gray (east of Beichuan) are known to be Mesozoic in age. City abbreviations (in white) are B, Beichuan; C, Chengdu; L, Lushan; M, Maowen; P, Pingwu; T, Tianquan; W, Wenchuan; Y, Yingxiuwan; Z, Zicheng.

[10] We examine channel gradients along rivers draining the eastern margin of the Tibetan Plateau adjacent to and north of the Sichuan Basin (Figure 1). All of these rivers are moderate size (<200 km in length), steep bedrock channels (see below) whose headwaters rise at ~4000 m on the Tibetan Plateau. All eventually drain across the Sichuan Basin into the Yangtze River, and thus have experienced similar base level histories. Our analysis relies primarily on channel profiles extracted from a digital elevation model [see *Fielding et al.*, 1994] but is guided by field observations along select channels.

4. Theoretical Framework

[11] Incision by rivers into bedrock can be limited by the detachment of intact bedrock [e.g., *Howard*, 1994] or by the capacity of the channel to transport the sediment load [e.g., *Tucker and Slingerland*, 1996; *Willgoose*, 1994]. In either case, incision is typically modeled as a power law function of contributing drainage area (as a proxy for discharge) and local channel gradient [*Howard*, 1994; *Howard and Kerby*, 1983; *Moglen and Bras*, 1995; *Willgoose*, 1994]. For illustrative purposes, we will utilize the detachment-limited case [*Howard et al.*, 1994], but we note that the analysis is readily applicable to transport-limited conditions. In studies where the transient response of channel profiles to temporal changes in climate, base level, or tectonics is a primary concern, the distinction between detachment-limited and transport-limited assumes greater importance [*Whipple and Tucker*, 2002].

[12] The evolution of a detachment-limited river profile is governed by the competition between rock uplift (relative to a fixed base level) and erosion rate, such that

$$\partial z/\partial t = U(x,t) - KA^m S^n, \quad (1)$$

where dz/dt is the time rate of change of channel bed elevation, U is rock uplift rate, K is a dimensional coefficient of erosion, A is upstream drainage area, S is local channel gradient, and m and n are positive constants that reflect basin hydrology, hydraulic geometry, and erosion process [*Howard et al.*, 1994; *Whipple et al.*, 2000a; *Whipple and Tucker*, 1999]. In particular, this formulation follows a typical derivation of stream power per unit bed area [*Whipple and Tucker*, 1999] by considering that the relationships between channel width and discharge and between discharge and drainage basin area are adequately described by power law functions.

[13] A number of researchers have recently argued that the incision rate in bedrock channels is a function of the ratio of sediment flux, q_s, to sediment carrying capacity, q_c [*Sklar and Dietrich*, 1998, 2001; *Slingerland et al.*, 1997]. A simple way to represent this dependence is to write

$$K = K' f(q_s, q_c), \tag{2}$$

where $f(q_s, q_c)$ is an unspecified function of sediment and water flux and K' is a dimensional coefficient that encapsulates the dependence of erosion rate on rock mass quality and erosion process [*Whipple and Tucker*, 1999]. *Sklar and Dietrich* [1998] argue that sediment flux plays a dual role in influencing incision rates by (1) accelerating erosion by increasing the number of tools in the flow and (2) inhibiting erosion by partial shielding of the bed from particle impact. For the purposes of developing a channel gradient index, we frame the problem with the simplest case where the influence of sediment flux is adequately captured by the downstream changes in stream power (i.e., $f(q_s, q_c) = 1$). A comprehensive treatment of the topographic implications of sediment-flux-dependent river incision models is presented by *Whipple and Tucker* [2002].

[14] Under steady state conditions ($dz/dt = 0$), with uniform U and K and constant m and n, the equilibrium channel gradient (S_e) decreases as a power law function of drainage are according to the relation [*Flint*, 1974; *Moglen and Bras*, 1995; *Sklar and Dietrich*, 1998; *Snyder et al.*, 2000; *Tarboton et al.*, 1989]

$$S_e = k_s A^{-\Theta}, \tag{3a}$$

where

$$\Theta = m/n \tag{3b}$$

$$k_s = (U/K)^{1/n}. \tag{3c}$$

Note that Θ in equation (3) represents the rate of change of channel gradient with increasing drainage area, not streamwise distance, as is commonly measured [*Demoulin*, 1998]. We also emphasize an important distinction between the concavity index (Θ) and the intrinsic concavity of the system (set by the ratio m/n). The two parameters are only equivalent under the restrictive conditions of steady state channels experiencing uniform U and K along their length [*Snyder et al.*, 2000]. As discussed below, the concavity index of most natural streams can vary over a wide range, independent of the ratio m/n. Both the concavity index and the steepness index of a given reach are easily estimated from regression of channel gradient and drainage area [*Moglen and Bras*, 1995; *Seidl and Dietrich*, 1992; *Snyder et al.*, 2000].

4.1. Current Constraints on Model Parameters

[15] Field calibrations of bedrock channel incision models are relatively rate, due in large part to the difficulty of deconvolving the myriad influences subsumed in model parameters. From a theoretical basis, the slope exponent (n) has been argued to depend on the dominant erosion process and to vary between ~2/3 and ~5/3 [*Hancock et al.*, 1998; *Whipple et al.*, 2000a]. In a seminal study of rapidly eroding badlands, *Howard and Kerby* [1983] concluded that historic incision rates and patterns were consistent with incision rate linearly proportional to bed shear stress (e.g., $m \sim 1/3$, $n \sim 2/3$). More recently, *Kirby and Whipple* [2001] argued that the adjustment of steady state channel profiles to downstream changes in uplift rate across a growing fold in the Siwalik Hills of Nepal was consistent with n between ~2/3 and ~1. Historic incision on the Ukak River in Alaska is interpreted to best fit a model with n significantly less than 1 [*Whipple et al.*, 2000b]. Finally, *Royden et al.* [2000] have argued that the form of transient river profiles developed in crystalline rocks in the eastern Himalayan syntaxis imply $n > 1$. The functional relationship between incision rate and channel gradient (n) remains a critical research avenue.

[16] Estimates of the value of the erosion coefficient, K, are likewise limited, but appear to indicate that K may vary over ~4 orders of magnitude, depending primarily on lithology and regional climate [*Stock and Montgomery*, 1999]. In addition, *Snyder et al.* [2000] have presented evidence that K varies in concert with uplift rate in the King Range of northern California. These authors argue that enhanced orographic precipitation, combined with a threshold for channel incision, can explain this observed dependence, although a contribution from sediment flux and/or debris flows cannot be ruled out [*Snyder et al.*, 1999].

[17] The intrinsic concavity (m/n) of detachment-limited channels is set by the relationships that govern basin hydrology and channel hydraulic geometry and is thought to be independent of erosion process; theoretical considerations suggest that m/n should fall in a narrow range of values between 0.35 and 0.6 [*Whipple and Tucker*, 1999]. In the few field sites where the assumptions underlying equation (3b) appear to be satisfied (that is, bedrock channels are developed on relatively uniform substrate and are experiencing uniform uplift rate along their length), measured concavities yield estimates of m/n very near 0.45 [*Kirby and Whipple*, 2001; *Snyder et al.*, 2000; *Whipple and Tucker*, 1999]. Although the intrinsic concavity of transport-limited channels is not as well characterized, preliminary estimates of the concavity of transport-limited channels fall within the same range (0.3–0.6 [*Tucker and Whipple*, 2002; *Whipple and Tucker*, 2002]) and may be expected to depend strongly on the rate of downstream fining.

4.2. Topographic Implications

[18] The simple model presented above carries several important topographic predictions for equilibrium channel

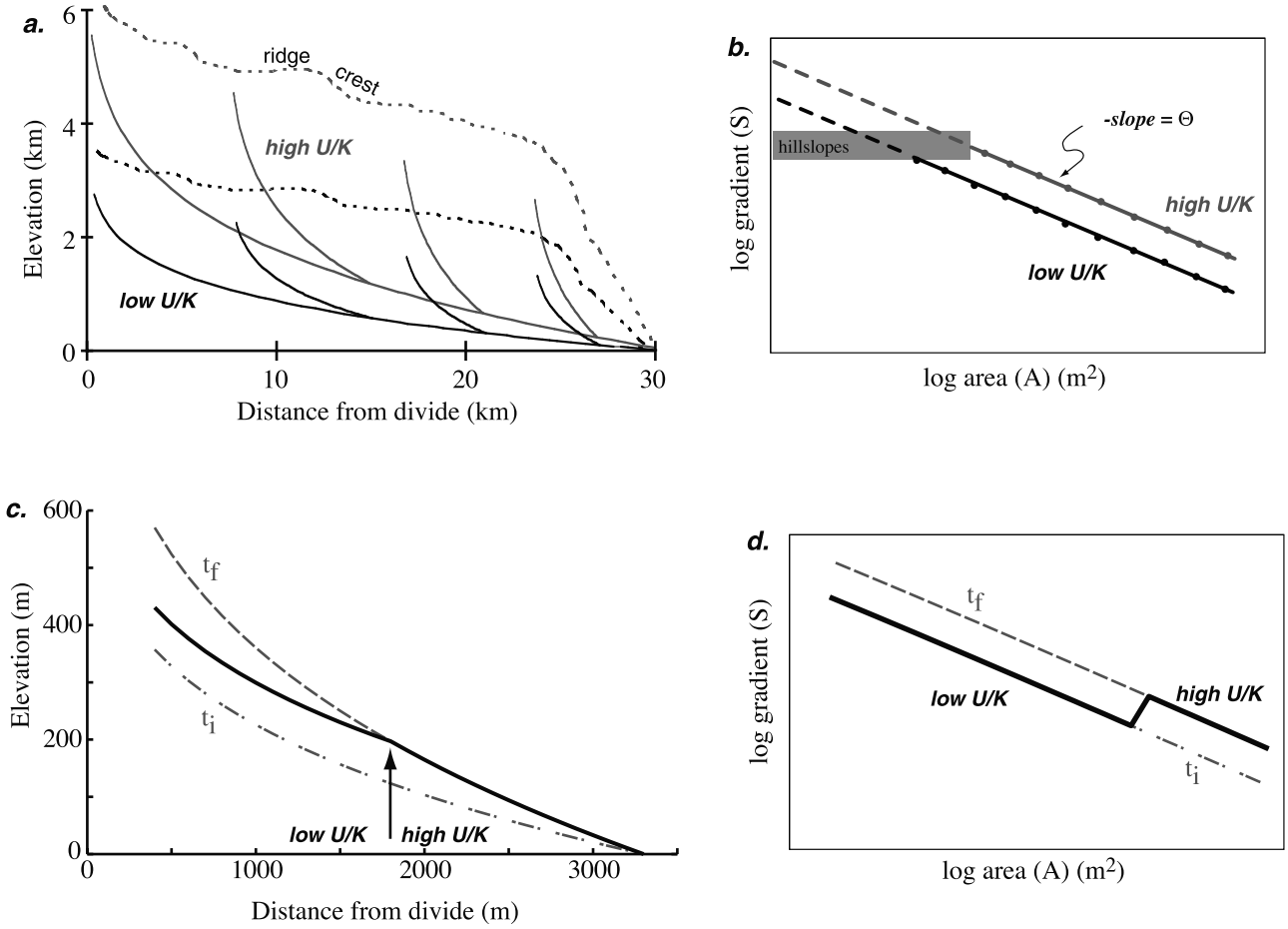

Figure 2. Schematic illustrations of channel response to differences in rock uplift rate and erosivity. (a and b) Topographic differences in steady state channels developed under conditions of uniform uplift and erosivity. Figure 2a is a longitudinal profile, and Figure 2b is a slope-area plot. Note that increases in uplift rate and/or decreases in erosivity result in steeper channels [e.g., *Whipple et al.*, 1999]. In so far as these changes are uniform along the channel, the concavity index remains the same. (c and d) Channels developed under nonuniform conditions. An increase in channel gradient approximately midway along the channel profile (arrow in Figure 2c) could be the result of an increase in local rock uplift rate, a more resistant lithology, or a transient response to base level fall (gray dashed lines represent an initial condition, t_i, and a final condition, t_f). In either case, the increase in gradient produces a distinct scaling break in slope-area space (Figure 2d).

gradients and their distribution in a tectonically active landscape. To a large degree these implications have been considered in detail previously [*Tucker and Whipple*, 2002; *Whipple and Tucker*, 1999, 2002]; we review selected aspects here to illustrate expected topographic patterns. Equation (3) implies that an equilibrium channel under conditions of uniform uplift and constant erosion coefficient should present a smooth longitudinal profile whose concavity is set by the ratio m/n and whose steepness is set by the coefficient $(U/K)^{1/n}$. Importantly, increases in rock uplift rate and/or decreases in erosive efficiency (a potential consequence of resistant substrate, bed protection by sediment, or decreases in discharge) result in steeper channels (Figure 2). However, in so far as these changes are uniform along the channel, the concavity index is unaffected.

[19] The argument that the ratio m/n is likely confined to a relatively narrow range does not necessarily imply that actual channel concavities (Θ) are likewise restricted. Any spatial variation in substrate competence [*Moglen and Bras*, 1995], erosive efficiency due to sediment flux [*Sklar and Dietrich*, 1998] or to orographic precipitation [*Roe et al.*, 2002], transient conditions [*Snyder et al.*, 2000], and/or differential rock uplift rate [*Kirby and Whipple*, 2001] will impact actual channel concavity. A simple example is illustrated in Figure 2. Here an increase in the steepness index (k_s) occurs midway down the channel and engenders a decrease in the concavity of the channel. Without a priori knowledge, this change in channel gradient might be interpreted as a local difference in lithologic resistance, an increase in uplift rate downstream, or the upstream extent of a transient wave of incision, or perhaps as the consequence of decreasing erosive efficiency due to sediment flux.

[20] Quantitative application of stream incision models is hampered by (1) uncertainty in the dependence of incision

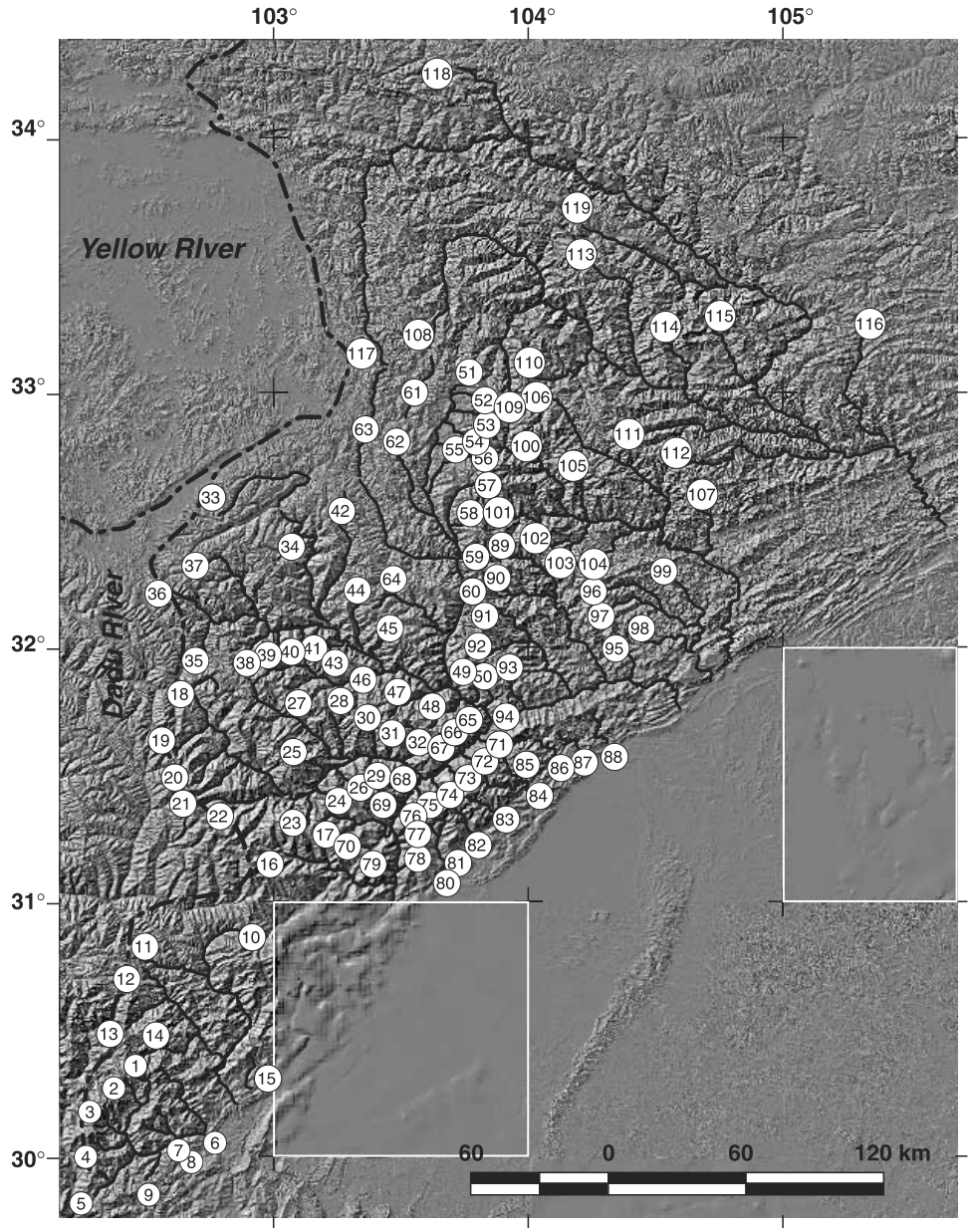

Figure 3. Index map of channels examined in this study. Numbers are keyed to Table 1 and are located near the headwaters of the channel (with the exception of channels 80–88, along the front of the Pengguan Massif). Heavy dashed lines show the positions of the major drainage divides between the dissected plateau margin and the Yellow and Dadu rivers. The background is a shaded relief image of the region. Illumination is from the west-northwest. White boxes highlight gaps in the digital elevation data (filled with GTOPO30 data).

rate on channel gradient (n in equation (1)) [*Whipple and Tucker*, 1999], (2) the degree of channel width adjustment to changes in rock uplift rate, (3) the extent and nature of upstream transitions to incision by debris flows, and (4) the uncertain role of sediment flux and armoring of the channel bed [e.g., *Sklar and Dietrich*, 1998]. Despite these complications, stream gradient analysis can still be a powerful tool for reconnaissance tectonic geomorphology. In this contribution, we examine relative differences in channel profile concavity and steepness in eastern Tibet and ask whether there are discernable spatial patterns in Θ and k_s. If so, we can begin to assess what range of processes described above may produce the observed patterns.

5. Stream Profile Analysis

[21] We examined 119 channels draining the eastern margin of the Tibetan Plateau between ~30°N and ~34°N (Figure 3). Topographic characteristics of the drainage basins are given in Table 1. The basins range in drainage area from ~20 km^2 to nearly 40,000 km^2. All

Table 1. Topographic Characteristics of River Profiles in Eastern Tibet[a]

Principal Channel	A_{min}, m^2	A_{max}, m^2	$\Theta \pm 2\sigma$	S_r ($A_r = 10^8$ m^2)	CSI ($\Theta = 0.4$)	Comments
			Qing Jiang, Upstream of Tianquan			
1	1×10^7	5×10^8	0.43 ± 0.04	0.063	97	
2	1×10^7	4×10^8	0.38 ± 0.03	0.052	89	
3	5×10^6	5×10^8	0.47 ± 0.03	0.086	142	
4	2×10^7	7×10^8	0.46 ± 0.04	0.061	102	
5	1×10^7	1×10^9	0.47 ± 0.03	0.044	64	
6	1×10^7	1×10^9	0.51 ± 0.04	0.058	97	
7	2×10^7	2×10^8	0.50 ± 0.05	0.052	95	
8	3×10^6	2×10^8	0.43 ± 0.03	0.058	92	
9	1×10^6	1×10^8	0.36 ± 0.03	0.032	48	
Mean			0.45 ± 0.05		92	
			Qingyi Jiang, Upstream of Lushan			
10	1×10^7	5×10^8	0.43 ± 0.03	0.053	85	upper reach
10	8×10^8	3×10^9	0.83 ± 0.11[b]	nc	92	lower reach
11	1×10^7	5×10^8	0.40 ± 0.03	0.048	77	
12	1×10^7	5×10^8	0.43 ± 0.03	0.059	104	
13	1×10^7	5×10^8	0.45 ± 0.03	0.068	100	
14	1×10^7	5×10^8	0.46 ± 0.03	0.057	101	
15	3×10^6	3×10^7	0.45 ± 0.09	nc	78	
Mean			0.44 ± 0.03		91	
			Yingxiuwan, Upstream of Yingxiuwan			
16	1×10^7	1×10^9	0.35 ± 0.02	0.068	117	glacial headwaters
16	2×10^8	2×10^9	0.47 ± 0.08	0.087	127	
16	1×10^7	1×10^9	0.39 ± 0.02	0.088	129	glacial headwaters
Mean			0.40 ± 0.06		124	
			Unnamed Tributary of Min Jiang, Between Yingxiuwan and Wenchuan			
17	1×10^7	6×10^8	0.44 ± 0.02	0.059	100	
			Tsakahao He, Upstream of Wenchuan			
18	4×10^6	2×10^{10}	0.28 ± 0.02[b]	0.035	68	includes Min Jiang
18	4×10^6	1×10^{10}	0.31 ± 0.03[b]	0.040	63	above Wenchuan
18	4×10^6	4×10^8	0.34 ± 0.04	0.032	51	headwater reach
19	3×10^6	3×10^8	0.43 ± 0.04	0.042	64	
20	3×10^6	3×10^8	0.44 ± 0.02	0.043	76	
21	1×10^6	1×10^8	0.34 ± 0.03	0.048	71	
22	2×10^6	2×10^8	0.42 ± 0.06	0.052	78	
23	5×10^6	6×10^7	0.48 ± 0.04	nc	135	
24	6×10^6	7×10^7	0.57 ± 0.06	nc	115	
25	5×10^6	6×10^7	0.50 ± 0.04	nc	133	
26	6×10^6	2×10^8	0.48 ± 0.03	0.076	124	
27	1×10^6	3×10^7	0.35 ± 0.05	nc	51	upper reach
27	3×10^7	4×10^8	0.21 ± 0.05[b]	0.063	92	lower reach
28	1×10^7	3×10^8	0.43 ± 0.05[b]	0.082	132	stepped profile
29	1×10^7	5×10^7	0.59 ± 0.06	nc	149	
30	5×10^6	1×10^8	0.40 ± 0.05	0.062	99	
31	5×10^6	6×10^7	0.33 ± 0.03	nc	158	
32	3×10^6	3×10^8	0.29 ± 0.02	0.081	113	
Mean			0.43 ± 0.09		101	
			Heishui He, Upstream of Maowen			
33	1×10^7	1×10^9	0.25 ± 0.07	0.020	30	upstream of granite
34	1.5×10^9	3×10^9	2.50 ± 0.56[b]	nc.	96	granite reach
35	4×10^6	3×10^{10}	0.33 ± 0.02[b]	0.037	70	includes Min Jiang
35	4×10^6	1×10^{10}	0.37 ± 0.03[b]	0.039	62	above Maowen
35	4×10^6	2×10^8	0.46 ± 0.03	0.034	59	headwater reach
36	1×10^7	7×10^8	0.48 ± 0.05	0.050	74	
37	1×10^8	5×10^8	0.40 ± 0.18[b]	0.067	98	stepped profile
38	1×10^7	2×10^8	0.43 ± 0.05	0.052	86	
39	6×10^6	7×10^7	0.45 ± 0.08	nc	100	
40	2×10^6	1×10^8	0.39 ± 0.03	0.066	98	
41	8×10^6	1×10^8	0.34 ± 0.06	0.069	102	
42	2×10^7	1×10^9	0.36 ± 0.05	0.036	57	
43	5×10^6	1×10^8	0.50 ± 0.04	0.061	109	
44	1×10^7	1×10^8	0.41 ± 0.08	0.047	77	
45	1×10^7	1×10^8	0.41 ± 0.05	0.077	135	
46	5×10^6	1×10^9	0.36 ± 0.04	0.050	79	
47	5×10^7	1×10^9	0.73 ± 0.13[b]	0.073	105	stepped profile
48	1×10^7	2×10^8	0.39 ± 0.05	0.076	112	
49	5×10^6	1×10^8	0.54 ± 0.03	0.037	74	southern Min Shan
50	2×10^6	3×10^8	0.57 ± 0.02	0.034	70	southern Min Shan

Table 1. (continued)

Principal Channel	A_{min}, m^2	A_{max}, m^2	$\Theta \pm 2\sigma$	S_r ($A_r = 10^8$ m^2)	CSI ($\Theta = 0.4$)	Comments
Mean			0.42 ± 0.08		84	
Mean (excludes 49, 50)			0.40 ± 0.07		86	
			Min Jiang, Upstream of Maowen			
51	1×10^6	4.5×10^9	0.36 ± 0.02[b]	0.025	40	fit above landslide
51	1×10^6	1×10^9	0.40 ± 0.02[b]	0.023	37	upper reach
52	2×10^6	1×10^8	0.57 ± 0.05	nc	44	Zhangla basin
53	5.5×10^6	1×10^8	0.50 ± 0.08	nc	48	Zhangla basin
54	7×10^6	1×10^8	0.58 ± 0.06	nc	51	Zhangla basin
55	1×10^7	5×10^8	0.68 ± 0.13	0.020	52	Zhangla basin
56	1×10^7	1×10^8	0.79 ± 0.06	nc	44	
57	8×10^6	2×10^8	0.63 ± 0.04	0.032	75	
58	1×10^6	5×10^8	0.40 ± 0.02	0.056	92	
59	5×10^6	1×10^8	0.44 ± 0.07	nc	80	
60	1×10^6	5×10^7	0.32 ± 0.03	nc	59	
Mean (52–60)			0.54 ± 0.14		61	
Mean (52–57)			0.62 ± 0.10		52	
61	5×10^6	3×10^8	0.32 ± 0.06	0.019	30	
62	7×10^6	4×10^8	0.39 ± 0.06	0.024	39	
63	5×10^6	5×10^8	0.27 ± 0.09	0.014	23	
64	4×10^6	1.5×10^8	0.49 ± 0.08	0.040	67	upstream of convexity
64	1.5×10^8	6×10^8	-0.37 ± 0.17[b]	nc	67	convex reach
Mean (61–64)			0.37 ± 0.09		40	
			Min Jiang, Downstream of Maowen			
65	3×10^6	5×10^7	0.47 ± 0.04	nc	98	west of W-M fault
66	2×10^6	4×10^7	0.28 ± 0.05	nc	91	west of W-M fault
67	2×10^6	1×10^8	0.24 ± 0.03	0.096	115	west of W-M fault
68	5×10^6	8×10^7	0.53 ± 0.04	nc	150	west of W-M fault
69	5×10^6	7×10^7	0.52 ± 0.04	nc	140	west of W-M fault
70	1×10^7	2×10^8	0.59 ± 0.03	0.056	102	west of W-M fault
Mean (65–70)			0.43 ± 0.13		116	
71	8×10^6	2×10^7	0.53 ± 0.11	nc	174	east of W-M fault
72	1×10^7	7×10^7	0.42 ± 0.05	nc	173	east of W-M fault
73	8×10^6	1×10^8	0.33 ± 0.06	0.096	137	east of W-M fault
74	4×10^7	2×10^8	1.3 ± 0.15[b]	nc	129	east of W-M fault
75	5×10^6	1×10^8	0.63 ± 0.04	0.070	150	east of W-M fault
76	5×10^6	5×10^7	0.57 ± 0.06	nc	121	Pengguan Massif
77	5×10^6	5×10^7	0.58 ± 0.07	nc	122	Pengguan Massif
78	5×10^6	4×10^7	0.45 ± 0.08	nc	109	Pengguan Massif
79	1×10^6	4×10^7	0.29 ± 0.03	nc	136	Pengguan Massif
Mean (71–79)			0.48 ± 0.12		139	
			Pengguan Massif, Eastern flank			
80	1×10^7	3×10^8	0.65 ± 0.03	0.055	95	
81	3×10^6	3×10^8	0.61 ± 0.02	0.056	109	
82	1×10^7	7×10^7	0.59 ± 0.05	nc	113	
83	1×10^7	1×10^8	0.58 ± 0.04	0.059	119	
84	3×10^6	2×10^7	0.62 ± 0.06	nc	111	upper reach
84	3×10^7	3.5×10^8	0.03 ± 0.08[†]	0.084	134	lower reach
85	5×10^6	1×10^8	0.44 ± 0.05	0.057	95	upper reach
85	1×10^8	3.5×10^8	0.18 ± 0.11[b]	0.075	135	lower reach
86	5×10^6	3×10^7	0.53 ± 0.07	nc	135	upper reach
86	3×10^7	2.5×10^8	0.28 ± 0.06[b]	0.050	84	lower reach
87	1×10^7	1.5×10^8	0.96 ± 0.06	0.023	62	
88	3×10^7	2×10^8	0.74 ± 0.16	0.020	38	
Mean			0.64 ± 0.14		97	
Mean (1–4)			0.57 ± 0.07		111	
			Jin Jiang, Southern Min Shan			
89	8×10^6	4×10^9	0.56 ± 0.03	0.045	67	entire profile
89	8×10^6	1×10^8	0.53 ± 0.05	0.044	87	upper reach
89	2×10^8	4×10^9	0.76 ± 0.07	nc	58	middle reach
90	1×10^7	4×10^9	0.62 ± 0.02	0.046	71	entire profile
90	1×10^7	1×10^8	0.65 ± 0.04	0.047	98	upper reach
90	2×10^8	4×10^9	0.78 ± 0.08	nc	51	middle reach
91	3×10^6	4×10^9	0.60 ± 0.03	0.046	78	entire profile
91	5×10^6	2×10^8	0.39 ± 0.03	0.049	84	upper reach
92	3×10^6	1×10^8	0.56 ± 0.02	0.049	105	upper reach
92	1×10^8	4×10^9	0.78 ± 0.10	nc	55	middle reach
93	8×10^6	5×10^8	0.56 ± 0.03	0.044	70	
94	5×10^7	4×10^9	0.62 ± 0.08	0.037	57	survey branch
95	5×10^6	5×10^8	0.41 ± 0.07[b]	0.025	39	

Table 1. (continued)

Principal Channel	A_{min}, m^2	A_{max}, m^2	$\Theta \pm 2\sigma$	S_r ($A_r = 10^8$ m^2)	CSI ($\Theta = 0.4$)	Comments
Mean (entire reach)			0.61 ± 0.05		72	
Mean (upper reach)			0.52 ± 0.09		101	
Mean (lower reach)			0.78 ± 0.05		53	
			Unnamed Tributary of Fu Jiang, Eastern Min Shan			
96	1×10^7	1.5×10^9	0.74 ± 0.05	0.025	41	
97	1×10^7	1×10^9	0.74 ± 0.04	0.026	48	
98	1×10^7	1×10^8	0.58 ± 0.05	0.012	29	
98	1×10^8	2×10^8	−1.60 ± 0.59[b]	nc	43	convex reach
99	2×10^6	7×10^7	0.41 ± 0.04[b]	0.022	39	
Mean			0.69 ± 0.08		39	
			Fu Jiang, Central Min Shan			
100	5×10^6	3.5×10^8	0.42 ± 0.04	0.041	63	above knick zone
100	3.8×10^8	7×10^8	0.37 ± 0.29	0.105	171	Knick zone
100	8×10^8	7×10^9	0.91 ± 0.16	nc	42	below knick zone
101	2×10^7	7×10^9	0.70 ± 0.03	0.086	86	entire profile
101	2×10^7	4×10^8	0.45 ± 0.05	0.102	131	upper reach
101	4×10^8	7×10^9	0.81 ± 0.11	nc	47	middle reach
102	2×10^7	1×10^8	0.83 ± 0.07	0.039	85	
103	1×10^7	2×10^8	0.48 ± 0.04	0.046	83	
104	1×10^7	5×10^7	1.50 ± 0.17	nc	58	upper reach
104	5×10^7	1×10^9	0.43 ± 0.13	0.025	36	lower reach
105	1×10^7	2×10^8	0.56 ± 0.04	0.043	79	
106	1×10^7	5×10^8	0.53 ± 0.05	0.035	61	above knick zone
106	6×10^8	2×10^9	1.40 ± 0.32	nc	102	below knick zone
107	1×10^6	5×10^7	0.38 ± 0.04	nc	84	upper reach
107	5×10^7	2×10^8	1.20 ± 0.10	0.030	62	lower reach
Mean			nc		nc	
			Baishui Jiang, Northern Min Shan			
108	5×10^7	5×10^9	0.13 ± 0.04	0.018	58	upper reach
108	7×10^9	6×10^{10}	0.77 ± 0.34	nc	33	lower reach
109	5×10^6	2×10^9	0.32 ± 0.02	0.047	75	
110	1×10^7	7×10^8	0.61 ± 0.06	0.057	74	
111	1×10^7	6×10^8	0.67 ± 0.03	0.005	78	
112	8×10^6	7×10^7	0.40 ± 0.05	nc	101	upper reach
112	8×10^7	9×10^8	0.86 ± 0.07	0.046	49	lower reach
113	5×10^6	1×10^9	0.40 ± 0.02	0.037	59	
114	8×10^6	5×10^8	0.56 ± 0.03	0.045	81	
115	1×10^7	5×10^8	0.70 ± 0.04	0.045	69	
116	7×10^6	7×10^8	0.26 ± 0.04	0.017	33	
Mean			nc		nc	
			Bailong Jiang, Northern Min Shan			
117	4×10^7	1×10^9	0.25 ± 0.05	0.020	38	upper reach
117	1×10^9	1×10^{10}	0.45 ± 0.10	nc	67	middle reach
117	1×10^{10}	4×10^{10}	0.75 ± 0.49[b]	nc	41	lower reach
118	2×10^6	1×10^9	0.44 ± 0.03	0.041	63	
119	1×10^8	1.4×10^9	0.39 ± 0.05	nc	50	
Mean			0.38 ± 0.09		55	

[a] A_{min} and A_{max} refer to the minimum and maximum drainage areas, respectively, considered in the regression; nc, not calculated. The relative steepness (S_r) was not calculated for profile reaches outside the range of A_r. Note that mean concavities were not calculated for the Fu and Baishui drainages due to a wide range of values.

[b] Data excluded from mean where profile displayed distinct knickpoints or where systematic downstream changes in concavity occurred (e.g., eastern flank of the Pengguan Massif). See comments for details.

channels ultimately drain across the Sichuan Basin and join the Yangtze River in southeastern Sichuan Province.

[22] Channel elevations and upstream drainage areas were extracted from digital topographic data with a nominal resolution of 3 arc sec [*Fielding et al.*, 1994]. We removed spikes along the channel and smoothed the data using a moving average of 45 pixels. The window size was chosen to remove the high-frequency noise associated with the digital data, while retaining the general form of the profile. Implicit in the degree of smoothing is our attempt to only interpret long-wavelength (more than a few kilometers) changes in channel gradient. In order to test the reliability of channel profiles extracted from the digital data, we conducted detailed surveys of three selected channels (Hei Shui He, Jin Jiang, and Fu Jiang, Figure 1) and reconnaissance surveys along several of others (Baishui Jiang, Min Jiang, Tsakahao He). We surveyed channel elevation using a differential GPS (Jin) or altimeter readings corrected for changes in barometric pressure over the course of the survey (Hei Shui and Fu). Both survey techniques yielded channel profiles similar in form to those extracted from the digital data, including a steep knick zone along the upper reaches

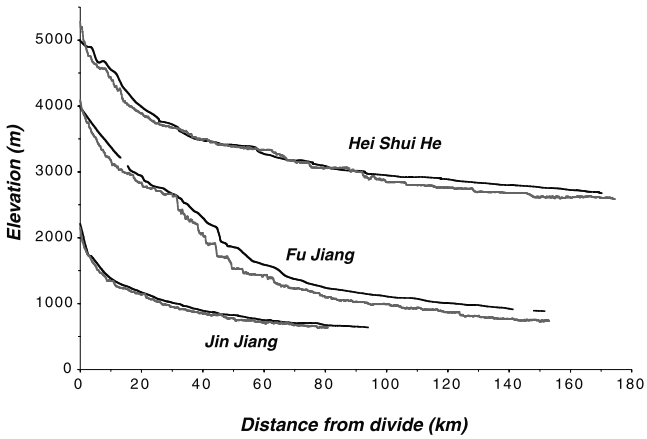

Figure 4. Comparison of longitudinal profiles extracted from digital elevation model (gray) and field surveys (black). Profiles shown are those of the Jin (channel 94), the Fu (channel 100), and the Hei Shui (channel 36, upstream of the city of Maowen). The profiles of the Hei Shui have been shifted by 1000 m for clarity. The general agreement between surveyed and extracted profiles indicates that the DEM adequately captures the general form of the channel.

of the Fu (Figure 4). Thus we are encouraged that the digital data appear adequate to capture the general form of longitudinal profiles in the region.

[23] We calculated channel gradients over a constant vertical interval of 10 m from the smoothed elevation data [e.g., *Snyder et al.*, 2000]. Regression of local channel gradient against upstream drainage area yielded estimates of the concavity and steepness indices (Θ and k_s, respectively). All regressions were limited to the fluvial channel and excluded data from the hillslopes and colluvial channels [*Montgomery and Foufoula-Georgiou*, 1993; *Snyder et al.*, 2000; *Tarboton et al.*, 1989]. Regressions extend downstream to the Sichuan Basin (in the case of the largest rivers) or to the junction with the main stem (in the case of tributaries). In all cases, where we observed obvious breaks in the gradient-area scaling trends, we performed regressions on each segment independently.

[24] In principle, the regression coefficient (k_s) is similar to the stream gradient index [*Hack*, 1973] but allows for a more general evaluation of profile steepness, independent of the form of a model profile. However, given the strong covariance of regression intercept (k_s) with the slope of the regression (Θ), comparison of steepness indices can be problematic [e.g., *Sklar and Dietrich*, 1998]. In order to effect a meaningful comparison of mean river gradient among channels having different drainage areas and different concavities, we utilized two different measures of channel steepness. First, we follow *Sklar and Dietrich* [1998] in normalizing by a representative area (A_r) in the center of the range of area data (here taken as 10^8 m^2) to obtain a representative slope (S_r), which describes the relative steepness of the profile reach:

$$S = S_r(A/A_r)^{-\Theta}. \quad (4)$$

Given the wide range of drainage areas we considered, however, this technique was applicable to only a limited number of channels. Consequently, we also determined the regression intercept, k_s, for all channels using a fixed regression slope (in this case, 0.4). This method also effectively removes the dependence on profile concavity and provides an alternative means of comparing channel steepness [*Snyder et al.*, 2000]. We refer to this measure as the normalized channel steepness index (CSI) in order to distinguish it from the regression intercept, k_s. Although our choice of reference concavity (0.4) reflects our argument that m/n is expected to fall near this value, we note that any choice of regression slope will effect a relative comparison of channel steepness. Effectively, the parameter provides a measure of the weighted mean of channel gradients within any given reach (Figure 4).

[25] Glaciated drainage basins typically have profiles that display dramatically different concavities from fluvial basins [*Brocklehurst and Whipple*, 2002] and would complicate our analysis. Although glaciated regions occur in the headwaters of some channels near the drainage divide with the plateau, we only observed distinct glacial morphology of channel profiles in a few headwater reaches along the eastern margin of the plateau. Field observations along several of these channels (Hei Shui He, Min Shan, Figure 1) revealed small terminal moraines between 4000–4500 m above mean sea level. For the purposes of this paper, drainages with obvious glacial morphology are excluded from consideration.

6. Results

[26] Taken as a whole (Table 1), our results demonstrate that channels in eastern Tibet display a wide range of concavity indices (Figure 5a), varying from near linear ($\Theta \sim 0$) to highly concave ($\Theta \sim 1.5$) profiles. However, the majority of these values fall between near 0.5 (mean of 0.5 ± 0.2) and suggest that to first-order, channel concavities in this landscape are similar to those determined under conditions of uniform uplift rate and erosivity. Normalized channel steepness indices also vary widely, from $\sim$20 to $\sim$180, indicative of strong variability in mean channel gradients in this landscape. Importantly, a comparison of our normalized channel steepness index with the representative slope method [*Sklar and Dietrich*, 1998] of evaluating mean channel gradients demonstrates that both provide a similar gauge of relative differences in mean channel gradient among profiles (Figure 5b). As discussed below, these variations in channel concavity and steepness are intimately related, and show a strong geographic distribution with respect to the topographic margin of the plateau. These geographic differences are significant and feature prominently in our eventual interpretation of the controls on channel topography. We first discuss concavity indices and then turn our attention to normalized steepness indices.

6.1. Concavity

[27] We assigned the concavity index derived from regression of channel gradient and drainage area data to the length of the channel encompassed by the regression interval to develop a map of the spatial distribution of

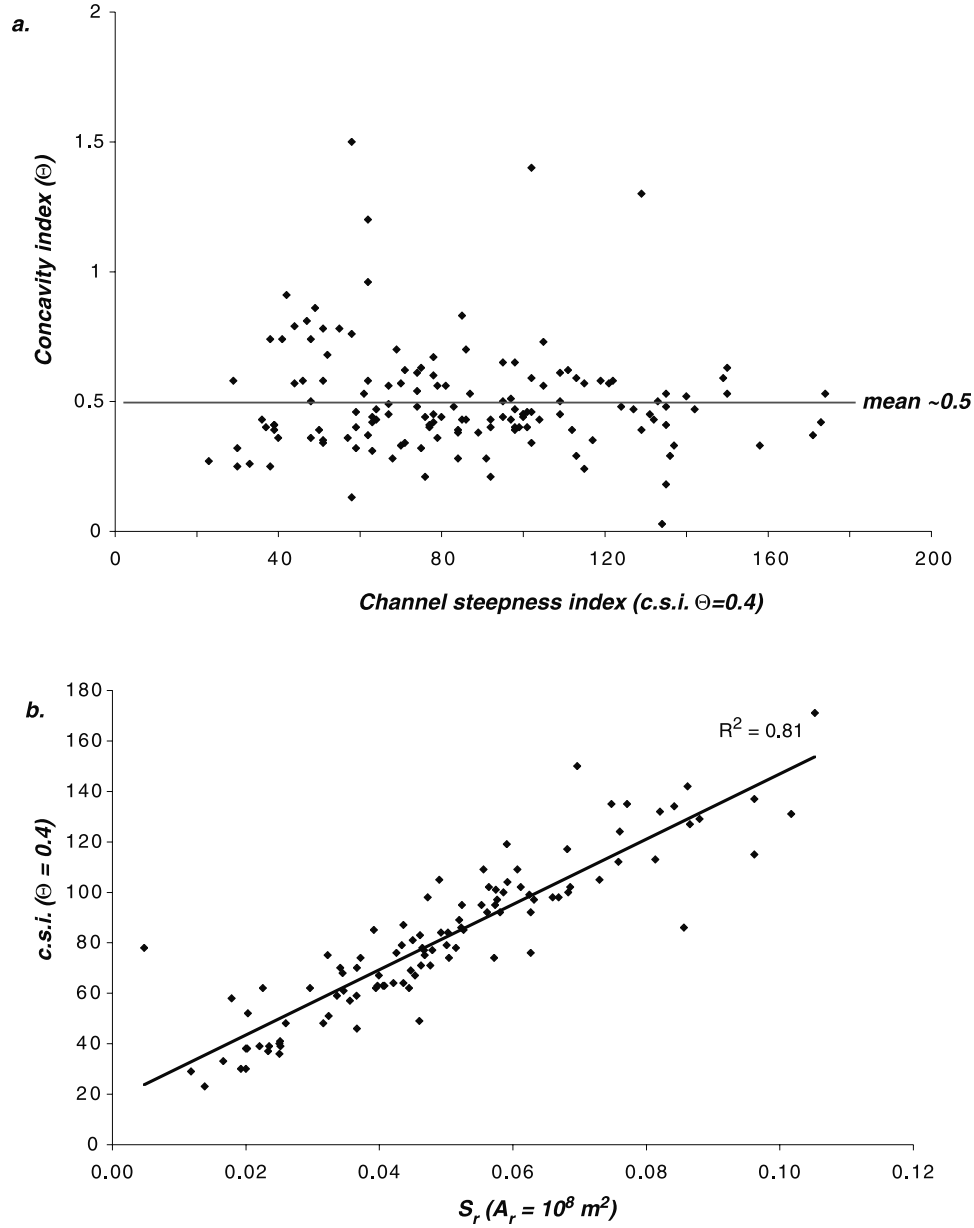

Figure 5. Methods of normalizing channel gradient in eastern Tibet. (a) Channel steepness index (CSI) calculated for a fixed concavity ($\Theta = 0.4$) plotted against the concavity of the profile (Θ). Data for two negative values (convex upward) are not plotted. (b) Comparison of representative slope (S_r) and steepness index (CSI) methods of determining relative channel steepness.

concavity indices (Figure 6). We observe three modes of channel concavities that appear to be related to the geographic position of channels relative to the topographic margin of the plateau. We discuss each of these regions independently: (1) southern Longmen Shan (comprising the Qing/Qingyi basin, Figure 1), (2) central and northern Longmen Shan (including the Min Jiang and its major tributaries, the Hei Shui He and Tsakahao He), (3) the eastern Min Shan (Fu/Jin drainage basins, Figure 1), and (4) the northern Min Shan (Bailong/Baishui basins, Figure 1).

6.1.1. Southern Longmen Shan

[28] The southern Longmen Shan is drained by the Qing Jiang and its major tributary, the Qingyi Jiang (Figure 1). These basins are relatively small, and the drainage divides are set by a competition with tributaries of the Dadu Jiang, a major N-S river to the west. The headwaters of the Qingyi rise in Triassic greywacke and flysch of the Songpan-Garze terrane, cross a basement massif composed of Precambrian crystalline gneisses and granitoids, and then flow through a series of klippen composed of a Paleozoic passive margin sequence (carbonates and shallow marine clastics) and Mesozoic terrestrial deposits. Despite these fault-bounded, lithologic variations, we observe generally smooth profiles (Figure 7a) with nearly uniform concavities (mean $\Theta \sim 0.45$, Table 1 and Figure 6), consistent with the expectation for steady state channel profiles experiencing uniform uplift and rock resistance. An excep-

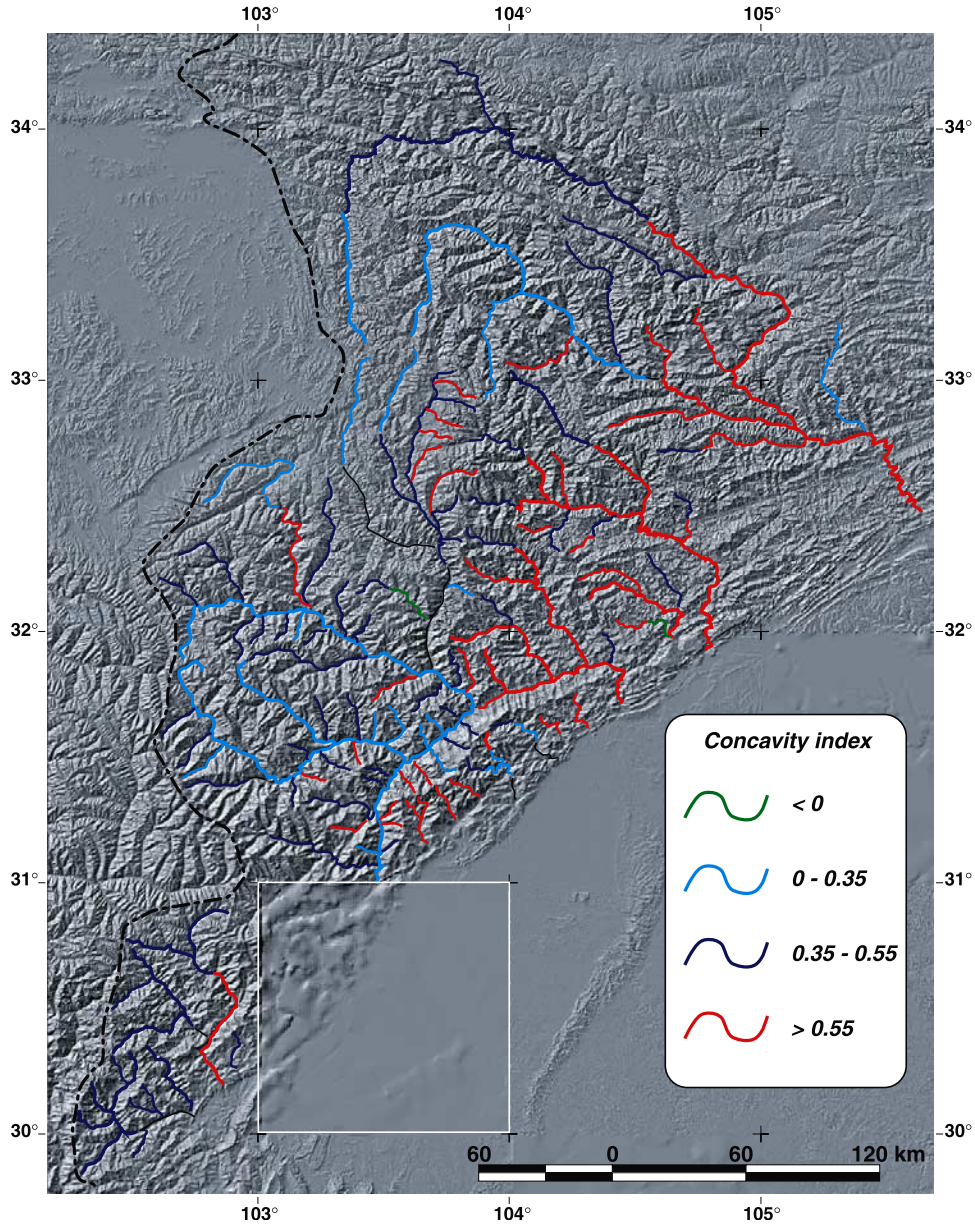

Figure 6. Map of concavity indices (Θ) determined for channels in eastern Tibet. Background is shaded relief image of the region illuminated from the west-northwest. White box represents region of gaps in data coverage (as in Figure 3). The approximate position of the drainage divide is shown as a heavy dashed line. Thin black lines represent portions of the channel network not analyzed because of data quality. Note that channels developed east of the Min Shan tend to have relatively high concavities (red), while those flowing from the plateau toward the margin tend to have low concavities (light blue).

tion occurs along the lower reach of the Qing Jiang, which displays a somewhat higher concavity (~0.8, Table 1).

6.1.2. Central Longmen Shan

[29] Most of the central portion of the study area is drained by the Min Jiang and its tributaries, the Hei Shui He and Tsakahao He (Figure 1). The Min Jiang drains a large region of the plateau west of the Min Shan range, turns southwest and flows along the Wenchuan-Maowen fault zone, and then crosses the Pengguan Massif to debauch into the Sichuan Basin west of Chengdu (Figure 1). The Hei Shui and Tsakahao rivers rise on the plateau some 150 km west of the Sichuan Basin and join the Min west of the Pengguan Massif. Both of these rivers begin in Triassic flysch and greywacke and cross a zone of greenschist grade metamorphics just west of the Wenchuan-Maowen fault [*Burchfiel et al.*, 1995; *Dirks et al.*, 1994].

[30] Note that we did not analyze the middle reach of the Min Jiang itself, north of the junction with the Hei Shui He (Figure 1). A massive landslide (>2 km^3) dammed the valley (at the junction of tributary 64, Figure 3) in the latest Pleistocene [*Kirby et al.*, 2000], and is still expressed as a ~200 m step in the channel profile extracted from the digital elevation model (DEM). Although the response of the Min to this local event is interesting in its own right, a

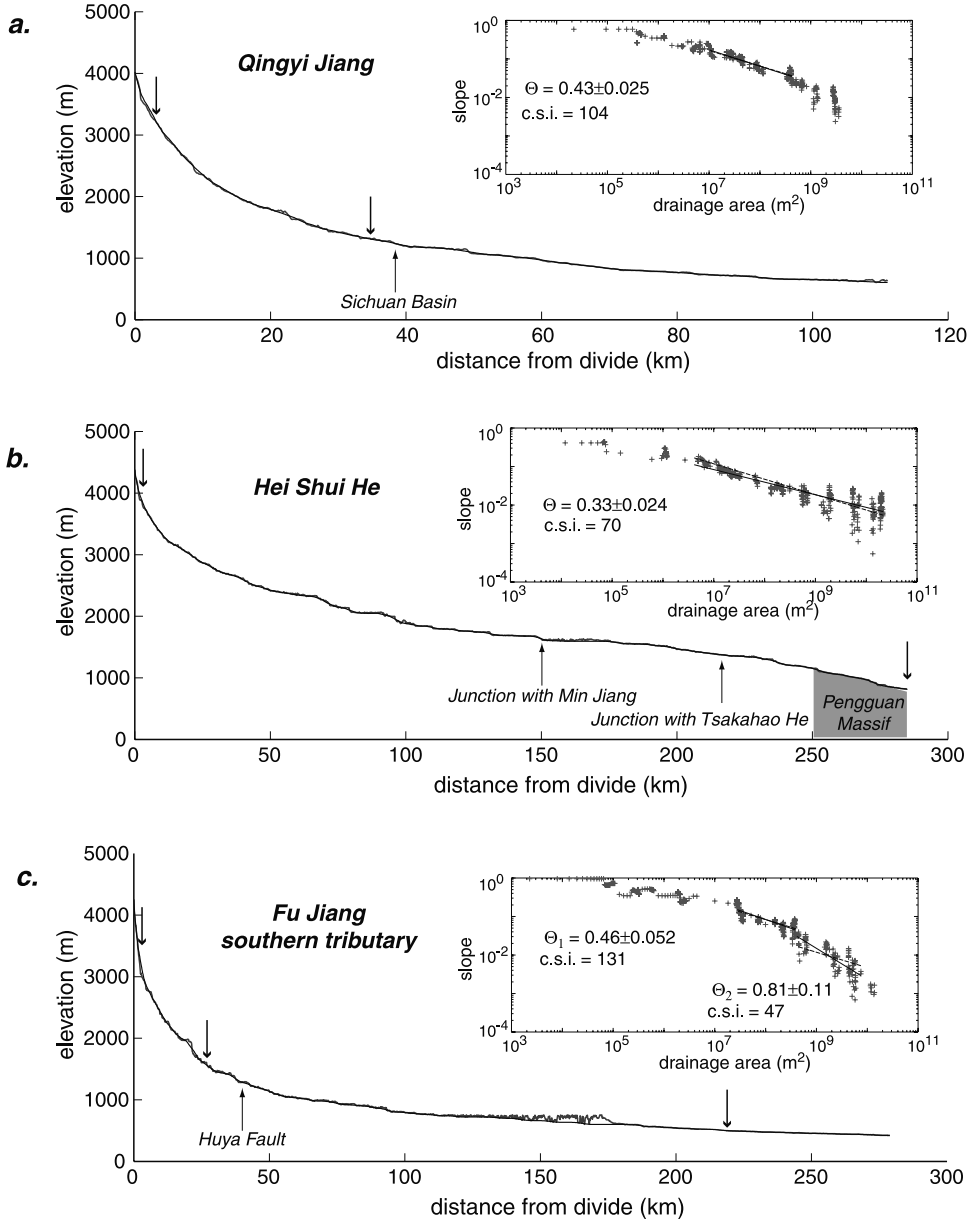

Figure 7. Channel profiles and gradient-area data for selected channels in eastern Tibet. For each, raw elevation data along the channel profile are shown in gray, while the smoothed and despiked data are shown in black. Gradients were calculated on a 10 m vertical interval (see text for details) and are plotted against upstream area for each channel (insets). Linear regressions of slope-area data are shown as black lines, while regression with fixed concavity ($\Theta = 0.4$) are shown as dashed lines. Arrows above the longitudinal profiles designate the region of channel elevations represented by the regression. Channel profiles are representative of (a) typical concavity (Qingyi Jiang, channel 12, Figure 3), (b) low concavity (Hei Shui He/Min Jiang, channel 35, Figure 3), and (c) high concavity (Fu Jiang, channel 101, Figure 3). Note that in Figure 7a, channel regression was truncated at margin of Sichuan Basin. Concavity index is slightly higher ($\sim$0.5) if regression includes all data. Also note in Figure 7c how the smoothed profile fits minima in a region of poor data quality. Key structures, geologic features, and major tributary junctions are shown for reference to the longitudinal profiles.

detailed analysis of this problem is beyond the scope of this paper.

[31] In general, tributaries of the Hei Shui He and Tsakahao He have concavities in the range of 0.4–0.5 (mean Θ of 0.42 and 0.43, respectively, Table 1). However, two important exceptions occur. First, the trunk streams of the Hei Shui He and Tsakahao He have relatively low concavities ($\Theta \sim 0.33$ and 0.28, respectively, Table 1 and Figure 6). Both rivers maintain steep gradients as they approach the Min Jiang where it parallels the Wenchuan-Maowen fault zone (Figure 7b). Downstream of the fault, the Min Jiang exhibits a broadly convex upward profile as

continues to increase gradient across the Pengguan Massif (Figure 5). The second exception occurs along the western flank of the Min Shan, where west flowing tributaries of the Min Jiang exhibit relatively high concavities ranging from 0.57 to 0.79 (Table 1 and Figure 6).

6.1.3. Eastern Min Shan

[32] In contrast to the Min Jiang, rivers that drain the eastern margin of the plateau north of the Sichuan Basin have their headwaters along the crest of the Min Shan and are generally characterized by high concavities (Figure 6 and Table 1). Several of the profiles appear to exhibit a scaling break from "typical" concavities (mean $\Theta \sim 0.52$) along the upper ~20 km of the channel to high concavities (mean $\Theta \sim 0.78$) along the lower reaches (Table 1 and Figure 7c), although the significance of this change remains uncertain.

[33] We include in this region a series of small channels draining the eastern flank of the Pengguan Massif (Figure 1). The massif is composed of Precambrian crystalline gneisses and granitoids separated from a series of Triassic mudstones by the Yingxiuwan-Beichuan fault zone (Figure 1). Channels in this region tend to have fairly complex profiles, characterized by moderately high concavities in the north and south. However, along the central portion of the massif, two channels display pronounced changes in concavity near the fault zone (Figure 6). Downstream of the fault, concavities are not well characterized due to a lack of data and are not represented on Figure 6.

6.1.4. Northern Min Shan

[34] The Bailong and Baishui rivers, like those along the Min, have their headwaters on the Tibetan Plateau (Figure 1). The upper reaches of both these rivers have relatively low concavities west of the Min Shan, while their middle reaches exhibit either a uniform concavity ($\Theta \sim 0.45$, Bailong) or low concavity ($\Theta \sim 0.13$, Baishui) as they cross the northern tip of the Min Shan (Figure 6). East of the topographic margin, however, both rivers display a downstream transition to higher concavities with Θ values near ~0.75 (Figure 6).

[35] In summary, we observe fairly systematic regional patterns in profile concavity that appear to be spatially associated with the topographic front of the plateau margin. Small tributaries typically have concavities within the expected range for steady state profiles undergoing uniform conditions along their length. However, the larger trunk streams that transect large regions of the plateau margin tend to deviate from these values. Rivers that have their headwaters on the plateau and flow toward the topographic front tend to have low concavities, while those that rise along the crest of the Min Shan and flow toward the foreland region tend to have high concavities.

6.2. Normalized Channel Steepness

[36] We derive a map of channel steepness indices (CSI) in the same fashion as concavities with one important difference. In the case where profile concavity differs substantially from the reference value, the CSI of a channel inferred from regression of the entire channel reach reflects only the mean gradient and contains little information about the variation of channel gradient along the reach. Consequently, for large rivers with concavities outside the expected range (e.g., Tsakahao He, Hei Shui He, Jin Jiang, Fu Jiang), we calculated the CSI over intervals of gradient-area data between major tributaries to capture the downstream changes in gradient implied by the concavity of the channels. For tributaries, the CSI was calculated between the channel head and the junction with the trunk stream.

[37] The resultant map of the CSI (Figure 8) reveals distinct spatial patterns in channel steepness across this margin of the plateau. A region of high-gradient channels (CSI ~ 90–100) exists near the margin of the Sichuan Basin (Figure 8) in the basin of the Qing Jiang and along the lower reaches of the Min Jiang. The zone of high-gradient channels continues north of the Sichuan Basin as a narrow region along the eastern flank of the Min Shan (CSI ~ 85–105, Figure 8). North of the Min Shan, the Baishui and Bailong maintain wide regions of increased gradient as they cross the plateau margin, although values are somewhat lower (CSI ~ 60–80, Figure 8), similar to tributaries in the upper part of the Hei Shui and Tsakahao basins.

[38] East and west of this zone of high channel gradients, channel profiles are systematically less steep (Figure 8). Rivers on the plateau, west of the Min Shan, have CSI values ~20–40, while those east of the range transition rapidly from high CSI values near the range crest to low values near the Sichuan Basin (Figure 8). Thus the high concavity of channels draining the eastern flank of the Min Shan is a simply measure of this relatively rapid downstream transition to low gradients. In a similar fashion, the low concavity of the Hei Shui He and Tsakahao He reflects an increase in CSI as the rivers approach the edge of the plateau (Figure 8). Tributaries near the headwaters of both rivers tend to have lower CSI values (~50–60) than those near the junction with the Min Jiang trunk stream (~100–150). There are a few exceptions along the upper Hei Shui He (Figure 8); these probably reflect a lithologic influence on channel gradient (see discussion below).

[39] Importantly, the increase in steepness index near the topographic front appears to be independent of drainage area. That is, both the main stem of the Min Jiang and its tributaries increase in CSI toward the plateau margin (CSI ~ 100–140, Figure 8). In the case of the trunk stream, this corresponds with a physical increase in gradient apparent in the longitudinal profile (Figure 7b). In the case of the tributary streams, channels are correspondingly steeper (at the same drainage area) toward the topographic margin of the plateau. Steepening of channels of all size relative to those farther west points to an external control on channel gradient that is independent of upstream drainage area.

7. Controls on Profile Gradient

[40] The zone of high stream gradients appears to coincide with the topographically highest portion of the plateau margin (Figures 1 and 8). This relationship reinforces suggestions that bedrock channels dictate much of the relief structure of tectonically active landscapes [*Whipple et al.*, 1999] and implies that the controls on channel gradient in this landscape ultimately dictate the topography and the relief along the margin of the plateau. In what follows we discuss the following potential influences on channel gradients: lithologic resistance, sediment flux, orographically induced variation in precipitation, transient response to changes in base level, and spatial variation in rock uplift.

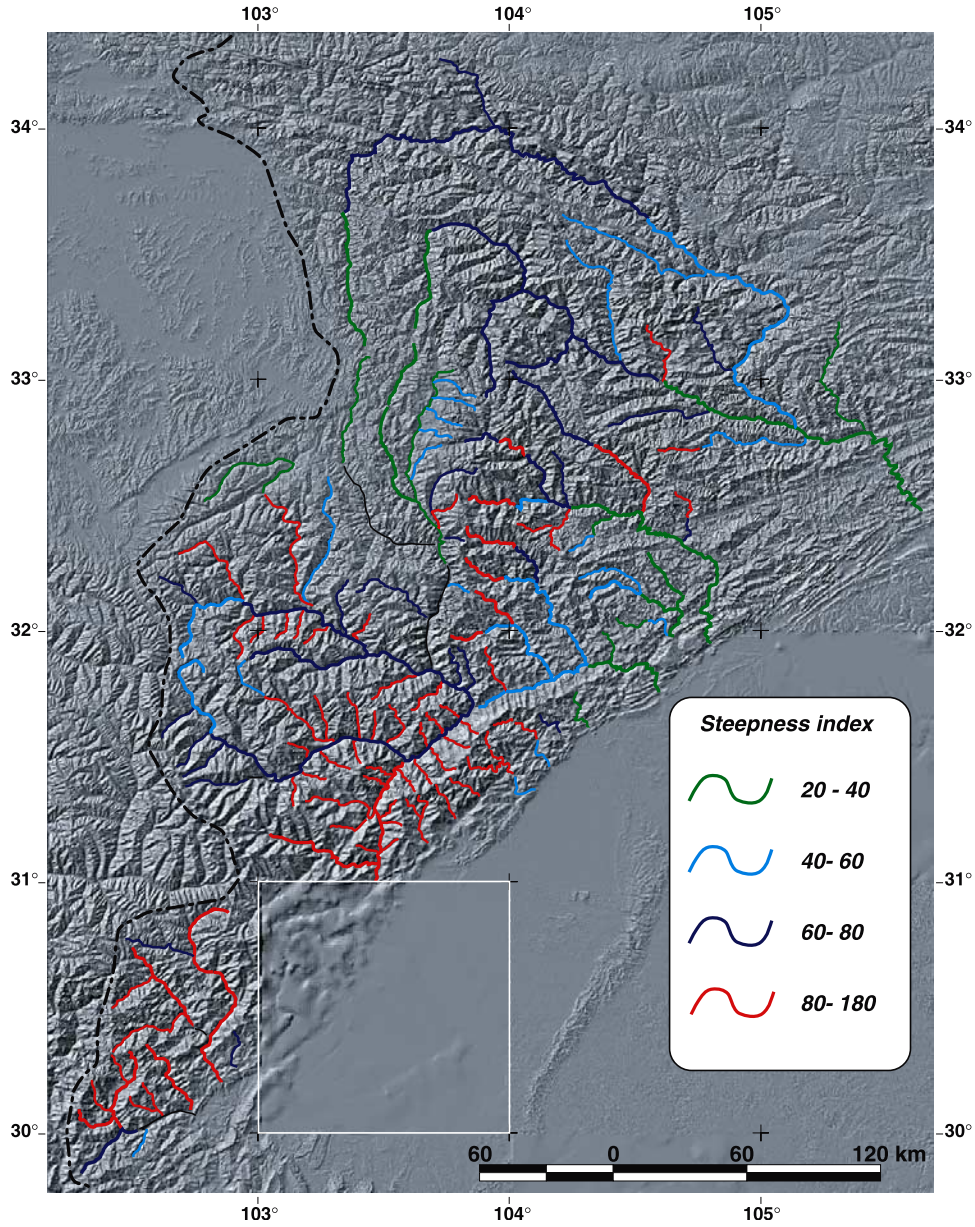

Figure 8. Map of steepness indices (CSI) determined for channels in eastern Tibet. Background as in Figure 3. Heavy dashed line represents the approximate position of the drainage divide. Note the high steepness indices adjacent to the topographic margin of the plateau.

For each, we qualitatively assess whether the observed pattern of channel gradient can be explained by the process in question.

7.1. Lithology

[41] It has been widely recognized that varying lithologic resistance to erosion can exert a strong control on channel gradient and landscape morphology [e.g., *Hack*, 19571973; *Moglen and Bras*, 1995; *Tucker and Slingerland*, 1996]. Recent calibration of a stream power incision model in regions of widely varying lithology yields estimates of the erosion coefficient (K) that vary over ~4 orders of magnitude [*Stock and Montgomery*, 1999]. Although differences in climate may account for some of this variation, it is clear that rock mass quality can significantly influence stream incision [*Sklar and Dietrich*, 1999; *Stock and Montgomery*, 1999]. In order to assess the potential role of lithologic resistance in influencing channel gradients in eastern Tibet, we compare the spatial pattern of CSI values determined from the topographic data with mapped variations in lithology (Figure 9). The geology was digitized from Chinese geologic maps at a scale of 1:200,000 [*Ministry of Geology and Mineral Resources*, 1991] and registered in a GIS database. In addition, we made qualitative observations regarding the competency of various lithologies (bedding planes, degree of jointing) during the course of our field investigations.

[42] In general, we see little influence of variable lithology on channel profiles. In the great majority of cases, changes in profile gradient (manifest as changes in the

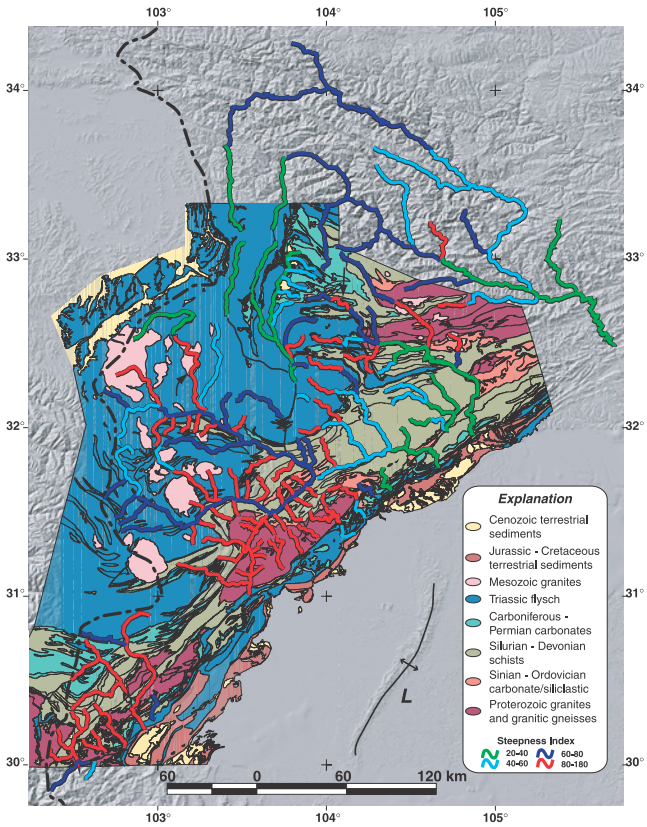

Figure 9. Comparison of channel steepness to lithologic variability in eastern Tibet. Geology was digitized from 1:200,000 Chinese geologic maps [*Ministry of Geology and Mineral Resources*, 1991] and updated from *Burchfiel et al.* [1995] and *Kirby et al.* [2000]. Note that the northern extent of the map reflects the extent of recent geologic mapping and of reliable information. Lithologic units are grouped according to relative competence. Large arrows highlight regions of distinct lithologic control on channel profiles as discussed in text. L, Longquan anticline. Heavy dashed line represents the position of the drainage divide.

slope-area arrays) do not correspond with mapped lithologic variations (Figure 9). For example, the two primary tributaries of the Qingyi Jiang, in the southern Longmen Shan (Figure 1), cross lithologies ranging from Triassic flysch to Precambrian gneisses and granites and yet show no discernable changes in gradient (Figures 7a and 9).

[43] In a similar fashion, the increase in gradient along the lower reaches of the Min Jiang and its tributaries (Hei Shui He and Tsakahao He) begins well upstream of the crystalline rocks of the Pengguan Massif, and appears to be distributed across a zone some 30–50 km wide (Figure 9) west of the Wenchuan-Maowen fault. East of the fault, there is a pronounced increase in the steepness index (Figure 9) which may be associated with the resistant rocks of the Pengguan Massif or may reflect a change in local uplift rate associated with active displacement on the W-M fault. In the field, we can discern little difference in apparent rock competence between the headwater reaches of these rivers (Triassic flysch) and the downstream reaches (Silurian-Devonian metasediments and Precambrian gneisses). Both are pervasively fractured and jointed at the meter to decimeter scale, and wholesale plucking of large blocks appears common.

[44] We do observe, however, a few channels where local changes in channel gradient coincide directly with lithologic differences. In general, these profiles are characterized by distinct convexities in the channel profile and corresponding steps in slope-area arrays (Figure 10). We discuss two of the most prominent, one of which occurs along the Fu Jiang in the eastern Min Shan and one which occurs in the upper Hei Shui He basin (highlighted on Figure 9 with arrows).

[45] Perhaps the best example of lithologic control of channel gradient occurs along the trunk stream of the Fu Jiang along the eastern flank of the Min Shan. The profile of the Fu displays a prominent convex section some 40 km downstream of the headwaters (Figure 10a) that coincides with a band of massively bedded, crystalline Pennsylvanian-Permian limestones (Figure 9). Steepness index (CSI) values along this reach are ~170, nearly three times that of the headwater region (Table 1). This stretch of channel runs in an extremely narrow gorge (in places <10 m) and is choked with massive boulders (10–15 m in diameter) and landslide debris that force the channel into steep cascades.

[46] The second example of lithologic influences on channel gradient occurs along the trunk stream of the Hei Shui He, upstream of the confluence between the northern and western tributaries (Figure 1). Here the channel displays a pronounced increase in gradient as it crosses a Mesozoic pluton (Figures 9 and 10b). The granite is characterized by a notable lack of jointing or foliation, and the channel is a narrow boulder cascade through this reach. Boulders range from 3 to 10 m in diameter along this section of channel. The increase in gradient imparts a high concavity to this reach of channel, while upstream of the granite, the concavity is quite low (Figure 6). Note that we chose regression intervals based on tributary junctions, not lithologic boundaries. Thus the high gradient inferred from the regression extends for some distance downstream of the granite (Figure 10b). Several other steep tributaries in the region cross similar plutons, and we suspect that many of the high gradient reaches along these tributaries can be singularly attributed to these plutons.

[47] In summary, although variable lithologic resistance can exert a strong control on channel gradients, in this landscape lithologic effects appear to be limited to local channel reaches, particularly those where rocks are massive and unjointed. This observation qualitatively supports inferences that erosion by plucking and block extraction is an efficient mechanism of channel incision [e.g., *Miller*, 1991; *Whipple et al.*, 2000a; *Wohl*, 1998]. However, lithologic variations do not appear to account for the systematic regional patterns in channel steepness indices.

7.2. Role of Sediment Flux

[48] During the course of our field work in eastern Tibet, we had the opportunity to qualitatively observe most of the major rivers in the region. Throughout the Longmen Shan and Min Shan, rivers are typically confined by steep, bedrock walls and intermittently expose bedrock in the channel floor (Figure 11a). Discontinuous strath terraces abound in the region and provide qualitative evidence for

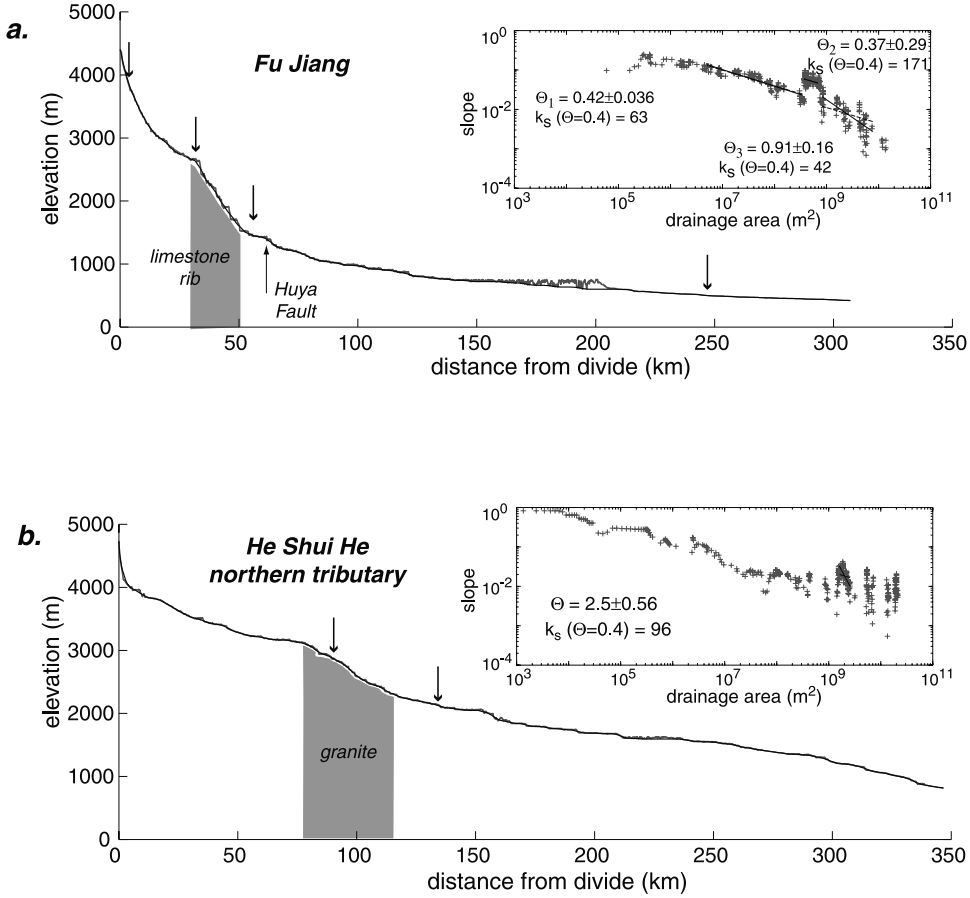

Figure 10. Selected examples of lithologic influence on channel gradient. Data are presented as in Figure 5. Grey band represents extent of resistant bedrock. (a) Trunk stream of Fu Jiang. Knick zone corresponds with rib of Pennsylvanian-Permian limestone. Note that profile smoothly crosses Huya fault. (b) Trunk stream of Hei Shui He. Knick zone corresponds with Mesozoic pluton and imparts a high concavity to the reach immediately downstream of granite.

recent incision. Many of the larger rivers, however, are mantled by a thin layer of cobble boulder alluvium along the bed and have hydraulic morphologies (e.g., constrictional rapids near tributary fans) typical of step pool and boulder cascade channels [*Montgomery and Buffington*, 1997]. Streambeds of smaller tributaries are often characterized by a lag of cobbles and boulders (Figures 11b and 11c). Thus many of the channels in the region are characteristic of "mixed" bedrock channels [*Howard*, 1998], but, as is typically the case, it is unclear whether this bed morphology reflects a long-term characteristic state, or whether the presence of sediment reflects the stochastic nature of sediment supply [*Howard*, 1998; *Massong and Montgomery*, 2000; *Slingerland et al.*, 1997]. In either case, it is clear that sediment flux could be an important influence on bedrock incision patterns in this landscape [e.g., *Sklar and Dietrich*, 1998].

[49] The effect of sediment flux on stream profiles depends critically on the functional form of equation (2). However, if we accept the premise of *Sklar and Dietrich* [1998] that incision rate, in general, should reach a maximum at some intermediate ratio of q_s/q_c, then we might expect that steady state channel profiles, developed under conditions of uniform uplift and lithology, would depart from a simple detachment-limited system in two significant ways. First, as erosion rates increase due to an increase in available tools, equilibrium channel gradients should decrease, imparting a high concavity to the upper portions of the channel network. Second, downstream reaches should display a relative increase in gradient (for a given area) as they are forced to steepen in order to maintain a constant erosion rate in the face of decreasing K as the bed is progressively protected from further erosion. The latter effect would reduce the concavity of the downstream reach relative to a detachment-limited model [*Whipple and Tucker*, 2002]. Of course, variations in grain size, mixed lithologies with varying rates of downstream communition [*Sklar and Dietrich*, 2001], and stochastic sediment delivery would impose additional complexities [*Sklar and Dietrich*, 1998].

[50] One might be tempted to interpret the increase in steepness index along the lower reaches of the Min Jiang and its tributaries as a response to increasing channel bed protection as sediment load increases [e.g., *Sklar and Dietrich*, 1998; *Slingerland et al.*, 1997]. However, we argue instead that the systematic patterns of channel gradient in eastern Tibet are not the result of downstream changes in sediment flux for two reasons. First, there does not appear to be a consistent relationship between profile

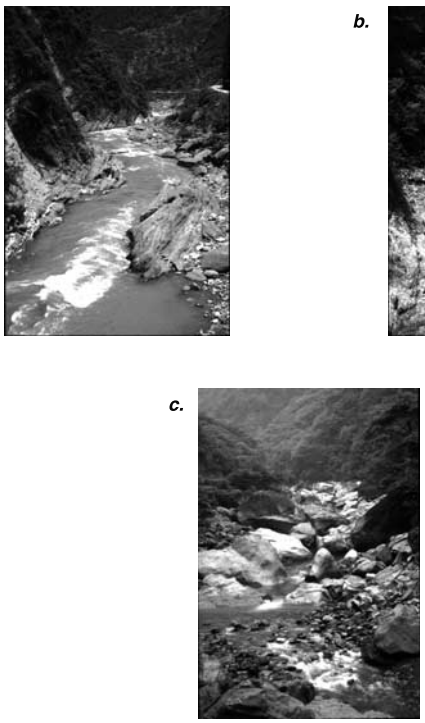

Figure 11. Photographs of channel bed morphology. (a) Trunk stream of the Jin Jiang, ~50 km above Beichuan (Figure 1). Note bedrock exposed in channel bottom and along both banks. A thin veneer of cobbles and boulders mantles the high-flow channel bed (at right). Channel is approximately 5 m wide. (b) Small tributary of Jin Jiang ~90 km above Beichuan. Channel is 3 m wide, and bed is mantled with cobbles and boulders throughout. (c) Tributary of Min Jiang, just upstream of Yingxiuwan (Y, Figure 1). Boulders up to 6 m in median diameter cover bed.

concavity and drainage area. While the Min Jiang and its tributaries begin to increase gradient between drainage areas of 10^8 and 10^9 m^2, those east of the Min Shan (Jin and Fu Jiang) continue to decrease in gradient at the same drainage area (Figure 12). Although appropriate combinations of sediment supply, lithologic competence, and rates of downstream fining could produce the observed patterns, such an argument begins to resemble special pleading. Second, tributaries of the Min Jiang drainage system show similar spatial variations in steepness index as the trunk streams (Figure 8). Tributaries near the headwaters of the drainage system have systematically lower CSI values than those near the topographic front (with the exception of those influenced by the distribution of Mesozoic granite plutons, as noted above). This pattern of CSI values further argues that high channel steepness is not drainage area-dependent. Rather, the strong geographic relationship of profile concavity to the plateau margin suggests to us that channel gradients in this landscape reflect an external forcing that is geographically restricted.

[51] We observe that steepness indices of tributary streams along the lower reaches of the Tsakahao He, above its junction with the Min Jiang (Figure 1), are systematically higher than the trunk stream (Figure 8). This mismatch between tributary and trunk stream CSI values persists for various reference values of Θ and does not appear to reflect uncertainty in the intrinsic concavity (m/n). It is possible that the difference in steepness between the trunk and tributary streams reflects a reduced erosional efficacy of these tributaries, perhaps due to protection of the bed by large boulders (Figure 11c). However, this effect does not explain the general increase in tributary CSI values from the plateau to near the topographic front (Figure 8). Thus, while sediment size and boulder competence may play a role in setting channel gradients along the small tributaries, the

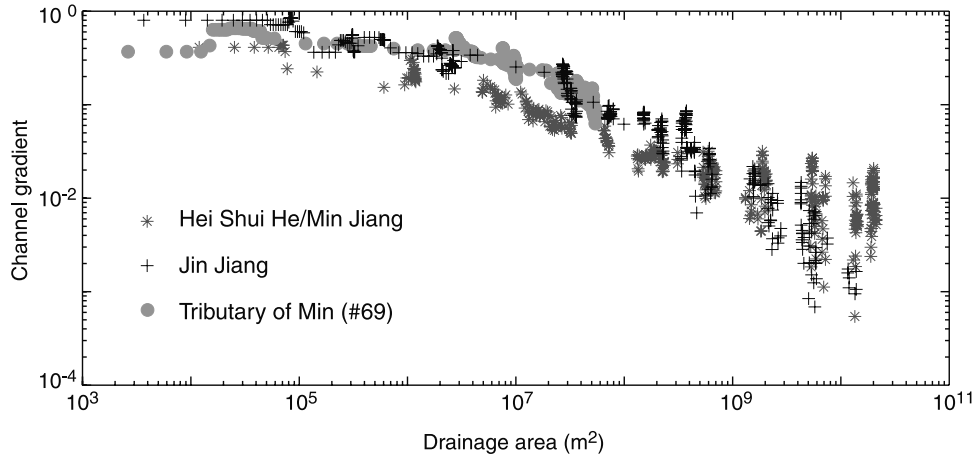

Figure 12. Comparison of gradient-area relationships for three drainages considered representative of regional variations in concavity. Note that the Hei Shui He/Min Jiang system displays a systematic relative increase in gradient at ~10^8 m^2, while the Jin Jiang continues to decrease in gradient at the same drainage area suggesting that regional differences in concavity are not related to downstream changes in sediment flux [i.e., *Sklar and Dietrich*, 1998]. Gradients in the headwater reaches of the Jin Jiang are similar to those along small tributaries of the lower Min Jiang and suggest an external control on channel gradient that we interpret to be active rock uplift.

general pattern of increasing steepness indices toward the topographic front appears to reflect an external control on channel gradients.

7.3. Orographic Precipitation

[52] The topographic front along the Sichuan Basin, coupled with the monsoonal climate of southwestern China, induces a steep gradient in precipitation across this margin of the plateau [*Fielding et al.*, 1994]. Mean annual precipitation varies from ~2 m/yr at the topographic front to slightly less than 1m/yr west of the drainage divide [*Korzoun*, 1977]. A simple consideration of a stream power incision rule, however, demonstrates that the increase in erosivity that might accompany greater precipitation along the front would be accompanied by a reduction in channel gradient [e.g., *Roe et al.*, 2002; *Whipple et al.*, 1999], as the river is more effective at balancing rock uplift. Although orographic precipitation may establish a potentially important feedback between climate and long-term denudation along this margin [e.g., *Willett*, 1999], the high gradients along the topographic front appear to be maintained in the face of greater precipitation.

7.4. External Controls on Channel Gradients

[53] We have argued to this point that the distribution of channel steepness indices in eastern Tibet reflects an external forcing that is geographically related to the topographic margin of the plateau. Increases in channel gradient typically reflect higher rates of long-term incision [e.g., *Kirby and Whipple*, 2001; *Snyder et al.*, 2000], although adjustments in channel hydraulic geometry can mitigate this relationship [e.g., *Lavé and Avouac*, 2000]. Although a detailed investigation of the distribution of channel incision rate in eastern Tibet is beyond the scope of this paper, preliminary studies support the inference that steeper channels are incising at greater rates. First, the steep lower reaches of the Min Jiang and Hei Shui He contain abundant evidence for recent incision in the form of discontinuous strath terraces (Figure 13a) and abandoned, incised tributary fans. In contrast, there is little evidence for recent incision along the upper reaches of the Hei Shui where tributary fans are graded to river level (Figure 13b) and strath terraces are markedly absent. These observations qualitatively suggest that the degree of recent incision into bedrock along the Hei Shui/Min system vary systematically with channel steepness. Second, in the eastern Min Shan, a similar relationship is borne out by incision rates inferred from radiocarbon and optically stimulated luminescence dating of strath terraces along the Jin and Fu rivers [*Kirby*, 2001]. Incision rates decrease toward the foreland, from ~3 mm/yr to less than 0.5 mm/yr, as channel gradients rapidly decrease east of the plateau margin (Figure 8). Thus we have some small measure of confidence that higher channel steepness indices in this landscape reflect higher rates of channel incision. However, the data are far too sparse to make any quantitative statements about the relation between incision rates and channel gradients (e.g., n in equation (1)) in this landscape. Rather, we focus on the mechanisms that could be responsible for the pattern of high channel steepness indices.

7.4.1. Base Level Fall

[54] With the exception of a small region west of the Longquan anticline (Figure 10), the Sichuan Basin is a heavily dissected landscape. Rivers draining across the basin to join the Yangtze have incised meanders ~100–200 m deep cut into Jurassic and Cretaceous mudstones that floor the basin. This incision appears to extend for some 500 km along the Yangtze River east from the Sichuan Basin (E. Kirby, unpublished data, 2001) and may represent a Quaternary base level fall along the Yangtze and its tributaries [*Li et al.*, 2001; *Zhao et al.*, 1997]. This wave of incision, however, does not extend west of the Longquan anticline, where the Min Jiang is actively depositing sediment on the Chengdu alluvial fan; it appears that the anticline has effectively isolated the Min Jiang and its tributaries from this base level signal. Thus recent base level changes cannot account for the steepening observed along the lower Min Jiang. Although base level fall could play an important role in influencing incision rates along the lower reaches of the rivers draining the Min Shan, we see no obvious sign of steepening in the lower reaches of channel

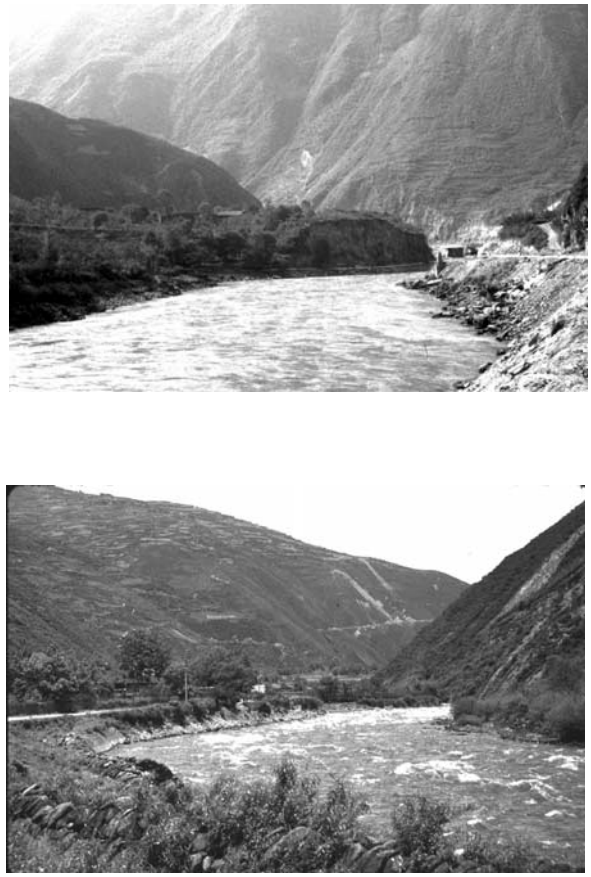

Figure 13. Photographs of variations in channel incision and local relief along the Hei Shui He/Min Jiang drainage. (a) Looking downstream along the lower Min Jiang (near Wenchuan, Figure 1). Strath terrace in midground is ~30 m above river level and is cut in Carboniferous limestone. Note impressive valley wall in background. Local relief along this stretch of river ranges from 3 to 4 km. (b) Looking upstream along the upper reach of the Hei Shui He. Note alluviated bed and lack of bedrock outcrop in bed and banks. Rapid is formed from a constriction at the terminus of a tributary alluvial fan (at left in midground). Local relief is ~500 m along this stretch.

profiles. Thus, if the signal has reached the margin of the plateau, it appears to have had a minor effect on channel gradients in the study area.

7.4.2. Escarpment Retreat

[55] In a companion study of the Cenozoic thermal history of the Longmen Shan and Min Shan, Kirby et al. [*Kirby et al.*, 2002] argued that the onset of rapid cooling in the late Miocene marked the initial development of the plateau margin in this region. Given the absence of active upper crustal shortening along this margin [e.g., *Chen et al.*, 2000], it is possible that the topography has been in a state of erosional decay since its initial development. The problem of escarpment retreat is fairly well studied [*Gilchrist et al.*, 1994; *Kooi and Beaumont*, 1994; *Tucker and Slingerland*, 1994] along passive margins, and we might expect that if the topographic margin had been retreating since the Miocene, channels would be steepest near the drainage divide and equilibrated in their downstream reaches, as observed along Gondawanan continental escarpments [*Seidl et al.*, 1996; *Weissel and Seidl*, 1998]. Such a pattern is inconsistent with the high gradients observed in the Min Jiang basin along the margin of the plateau adjacent to the Sichuan Basin. Although it is possible escarpment retreat could produce the pattern of stream gradients along the eastern flank of the Min Shan, independent evidence for rapid rock uplift within the range [*Kirby et al.*, 2000] suggests that high stream gradients near the range crest are tectonically controlled.

7.4.3. Rock Uplift

[56] Given the above arguments that lithology, sediment flux, orographic precipitation, and transient channel conditions cannot sufficiently explain the observed pattern of channel profiles, we reason that the spatial distribution of high stream gradients most likely reflects active rock uplift along the eastern margin of the plateau. Figure 14 schematically illustrates the spatial distribution of rock uplift that we infer from the distribution of channel steepness indices. Adjacent to the Sichuan Basin, the zone of high rock uplift appears to be distributed over a region $\sim$50–70 km wide parallel to the margin, while north of the basin, high rock uplift is apparently localized near the crest of the Min Shan. North of $\sim$33°N, rock uplift appears to be progressively distributed over a wider region of the margin.

[57] In our interpretation, the relatively high concavity of channel profiles along the eastern flank of the Min Shan (Jin and Fu Jiang) and the low concavity of the Min and Baishui systems reflect adjustments of channel gradient in response to these spatial variations in rock uplift rate along the plateau margin [e.g., *Kirby and Whipple*, 2001]. The slight break in gradient-area arrays observed along tributaries of the Jin Jiang (e.g., Figure 5c) may reflect somewhat more uniform uplift rates in the central Min Shan, but in general the high concavity of these systems likely reflects rock uplift rates that are decreasing from the range toward the Sichuan Basin. Note that several N-S tributaries in the region east of the Min Shan have concavities very near 0.4 (e.g., channels 95, 99, 104, 107, Table 1), consistent with the presence of E-W gradients in rock uplift (e.g., uniform uplift rates along the channels in a north-south direction). In a similar fashion, the gradual increase in gradient index (manifest as low concavity) along the Hei Shui He, Min Jiang, and Baishui Jiang reflects a relative steepening of these channels as they cross into the region of high rock uplift along the topographic front of the plateau.

[58] Although we cannot, at present, discern a quantitative relationship between channel gradient and rock uplift rate in this landscape, there are several lines of evidence that lend support to our argument that the distribution of channel gradients reflect underlying patterns in differential rock uplift. First, in a study of remnant Pleistocene basins, *Kirby et al.* [2000] documented rapid, west directed tilting along the western flank of the Min Shan (Figure 14). Differential rock uplift rates between the range crest and the plateau exceed $\sim$6 mm/yr. Small tributaries of the Min Jiang in this region exhibit relatively high concavities ($\sim$0.5–0.8, channels 52–56, Table 1), consistent with channels experiencing strong gradients in rock uplift. Second, fluvial incision rates inferred from Pleistocene-Holocene strath terraces in the eastern Min Shan [*Kirby*, 2001] decrease from $\sim$3 mm/yr in the core of the range to $\sim$0.5 mm/yr (Figure 14). Although the data are sparse, they are also consistent with decreasing incision rates toward the foreland region east of the Min Shan. Finally, long-term denudation rates inferred from thermochronology [*Kirby et al.*, 2002] suggest that rocks along the topographic margin of the plateau have experienced denudation rates on the order of 1–2 mm/yr since the late Miocene (Figure 14), while those farther west have experienced rates an order of magnitude lower over the same time interval (Figure 14). The long-term differences in denudation across this margin of the plateau are again consistent with the pattern of active rock uplift inferred from stream gradient analysis. Thus, while the quantitative relation between rock uplift and channel gradients remains uncertain, we conclude that differential rock uplift exerts a first-order control on channel profiles in this landscape.

8. Tectonic Implications

8.1. Discrete Versus Distributed Deformation of the Upper Crust

[59] Although there is a general correspondence between the zone of highest rock uplift and active faults in the region (Figure 14), one of the most intriguing results of this study is that we observe little direct influence of active faults on channel profiles. Rather the pattern of differential rock uplift that we infer from stream gradient analysis appears to be of a more distributed nature. In this section we consider the relationship of active faults to inferred gradients in rock uplift and explore the implications for the nature of upper crustal deformation in eastern Tibet.

8.1.1. Deformation in the Eastern Min Shan

[60] The nature of active deformation in the eastern Min Shan is somewhat enigmatic. Although the topographic front of the plateau in this region is coincident with a series of discontinuous en echelon, high-angle reverse faults (Huya fault and related structures, Figure 13), none of the faults appears to accomplish large-magnitude shortening of the upper crust, despite evidence for rapid tilting along the western range flank [*Kirby et al.*, 2000]. The lack of geodetically resolvable shortening across the Min Shan [*Chen et al.*, 2000; *King et al.*, 1997] suggests that strain

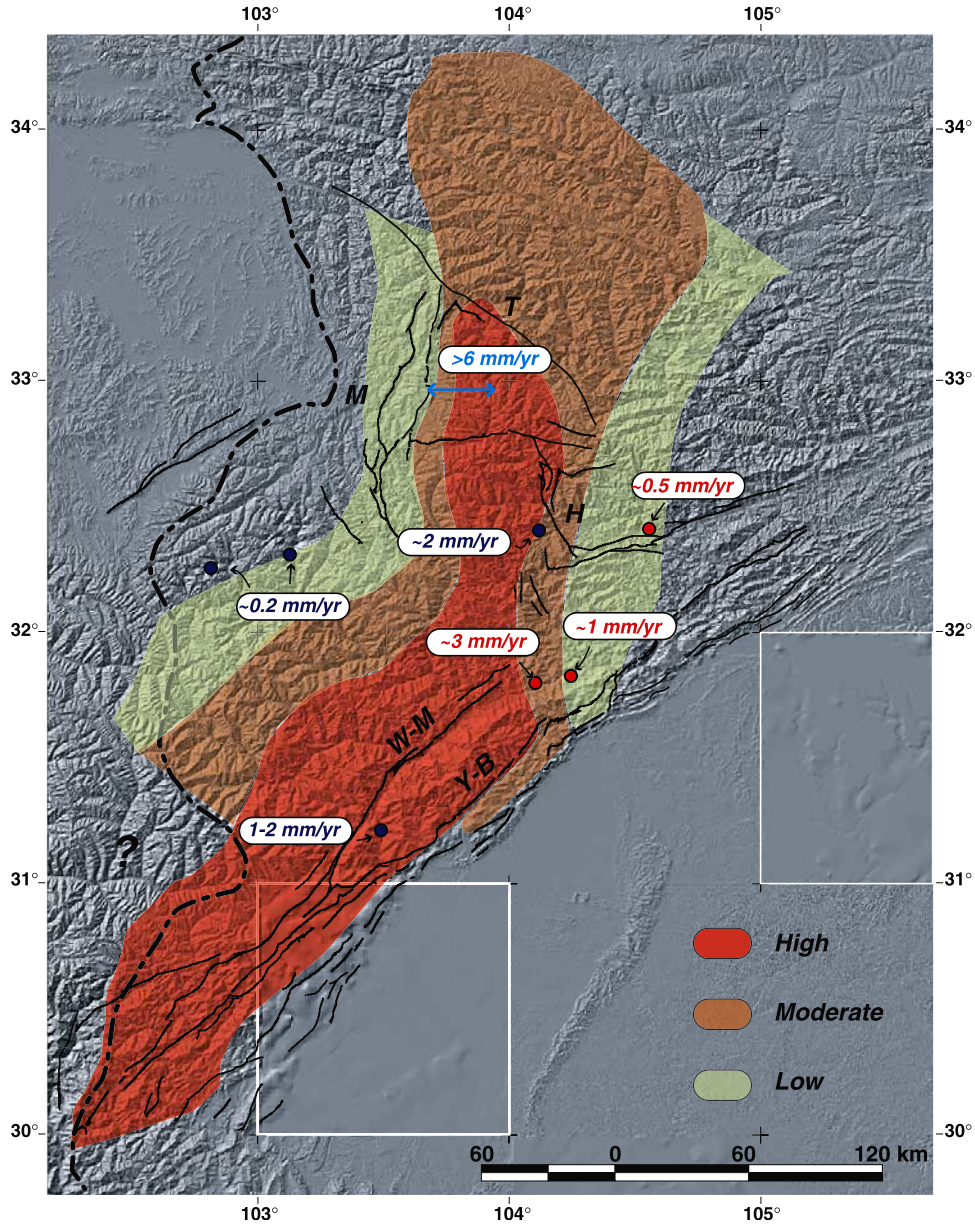

Figure 14. Schematic representation of the distribution of rock uplift inferred from channel profile steepness and its relationship to major structures in the region. Shown for comparison are fluvial incision rates (red) inferred from Pleistocene-Holocene terraces [*Kirby*, 2001], long-term denudation rates (dark blue) inferred from thermochronology [*Kirby et al.*, 2002], and rates of differential rock uplift in the western Min Shan (light blue) inferred from remnant Quaternary basins [*Kirby et al.*, 2000]. Note that all these measures are consistent with the pattern of active rock uplift inferred from stream gradient analysis. The position of the drainage divide is shown for reference as a heavy dashed line. Abbreviations are Y-B, Yingxiuwan-Beichuan fault zone; H, Huya fault; M, Min Jiang fault zone; T, Tazang fault; W-M, Wenchuan-Maowen fault zone.

accumulation in the upper crust is quite slow. Although the paleoseismicity of structures in the eastern Min Shan is unknown, the Chinese historic record suggests that the recurrence interval of large (magnitude > 5) events in this region is fairly long [*Editoral Board*, 1989]. Thus the presence of active rock uplift within the Min Shan [see also *Kirby et al.*, 2000] poses a question as to the manner by which rock uplift is accommodated along the eastern range flank.

[61] The region of highest channel gradients occurs west of the structures flanking the eastern range front, and it seems likely that they help to accommodate high rates of rock uplift within the range. However, two tributaries of the upper Fu Jiang cross the Huya fault with no significant disruption of channel profiles (Figures 10 and 11). The Huya fault is a steeply west dipping reverse fault [*Chen et al.*, 1994b] and is known to be active from a series of seismic events in 1976 [*Jones et al.*, 1984]. Both channels

are steeper to the west, in the hanging wall of the fault, but there is no discrete increase in stream gradient as would be expected for a discrete increase in rock uplift rate across the fault. Rather, the change in gradient appears to be distributed across a region some 20–30 km wide along the eastern flank of the Min Shan. As noted above, the high concavity of all the channels draining the eastern Min Shan display a similar pattern of changing channel gradients. We suspect that this reflects distributed rock uplift, although we cannot rule out the possibility that transport-limited conditions in the channels smooth the transition (see discussion below). If the former is correct, however, it implies that a significant component of active deformation in the eastern Min Shan may be accommodated by distributed tilting and/or pervasive shear of the crust, and that the active faults may not represent large-magnitude discontinuities in the deformation field.

8.1.2. Deformation in the Longmen Shan

[62] Active deformation in the Longmen Shan region is similarly complex. The topographic front of the plateau adjacent to the Sichuan Basin coincides with a number of regionally extensive thrust faults, first active in the Mesozoic, but possessing equivocal evidence for Quaternary displacements [c.f., *Burchfiel et al.*, 1995; *Chen et al.*, 1994b]. The pronounced increase in gradient observed along the lower reaches of the Min Jiang suggests that the Wenchuan-Maowen fault may mark an important uplift rate boundary. However, as noted above, the increase in gradient begins some 10km west of the active trace of the fault, and may suggest distributed differential rock uplift. In addition, we cannot readily separate potential lithologic and tectonic contributions to this increase in gradient east of the fault (within the Pengguan massif). At this point, we can only suggest that the fault may be active. In either case, differential rock uplift appears to be highest east of the fault zone, along the topographic front of the margin.

[63] Faults east of the Pengguan massif represent the most likely candidates for accomplishing differential rock uplift between the plateau and the Sichuan Basin. Streams draining the Pengguan Massif are quite steep west of the Yingxiuwan-Beichuan fault and maintain low gradients to the east. However, the fault also marks a pronounced lithologic transition from crystalline rocks to Triassic sediments, complicating the interpretation of channel gradients. Given the transition to depositional conditions in the adjacent Sichuan Basin, it seems likely that the Yingxiuwan-Beichuan fault accommodates active differential rock uplift along the margin of the Sichuan Basin.

8.1.3. Detachment Versus Transport Limited Conditions

[64] The lack of a discernable correlation between channel gradients and mapped lithologic changes, and between channel gradients and active faults, raises the possibility that many of these channels are transport limited. That is, their gradients may be set by the need to transport sediment supplied from upstream [*Tucker and Slingerland*, 1996]. Under these conditions, discrete step function changes in rock uplift and/or rock resistance may be distributed along the channel [*Whipple and Tucker*, 2002], as channel gradient responds to changing sediment input downstream. While we cannot confidently rule out this possibility, we note that geologic evidence for tilting in the western [*Kirby et al.*, 2000] and eastern Min Shan [*Kirby*, 2001] indicates that distributed deformation does occur within the region. In addition, transport-limited channel gradients will still reflect spatial variations in rock uplift, provided the systems are near steady state [*Willgoose*, 1994]. Thus, with the caveat that dynamic equilibrium may be difficult to prove in transport-limited channels [*Whipple and Tucker*, 2002], we believe that our inferences of the spatial distribution of rock uplift are fairly robust. However, until we develop a more complete understanding of the dynamics of bedrock channels in the region, the question of whether differential rock uplift in the eastern Min Shan is accomplished by discrete, localized deformation or is distributed over a broad region must rely on the limited geologic observations in the region [*Kirby*, 2001; *Kirby et al.*, 2000].

8.2. Tectonic Implications

[65] In general, active rock uplift in the absence of significant upper crustal shortening could be attributed to an isostatic response to flow in the upper mantle [e.g., *Molnar et al.*, 1993] or to thickening and flow within a weak lower crust [*Royden et al.*, 1997]. However, the spatial scale of the region of high rock uplift adjacent to and north of the Sichuan Basin (~20–40 km) implies that differential rock uplift is likely a response to crustal processes. Furthermore, the coincidence of this region with present-day high topography adjacent to the basin suggests that topography along the margin may be a direct reflection of this thickening. Although there is a general association of active faults with the zone of highest inferred rock uplift, active displacement on these structures is interpreted to be a relatively passive response to crustal thickening; the faults do not directly control the distribution of mountain building in this region [*Royden et al.*, 1997]. Indeed, the presence of spatial gradients in rock uplift rate east of the Min Shan suggests that deformation of the upper crust may be distributed over a region ~30–50 km wide. Enhanced resolution of these gradients would provide important constraints on the nature of upper crustal deformation in response to lower crustal thickening. We see this as strong motivation for high-resolution geodetic studies across this range.

[66] The distribution of rock uplift inferred from stream gradients also coincides roughly with the distribution of late Cenozoic denudation inferred from thermochronology [*Kirby et al.*, 2002]. The zone of highest stream gradients along the margin of the plateau coincides with a region of rapid late Miocene cooling inferred to reflect 8–10 km of denudation [*Kirby et al.*, 2002], while lower channel gradients on the plateau to the west coincide with older ages and slower cooling rates (Figure 14). Coincidence among the region of steepest channels, topographically high mountains along the plateau margin, and young cooling ages suggests a dynamic coupling between rock uplift, channel gradients, and long-term denudation during the topographic development of the eastern plateau margin. Perhaps the mechanical heterogeneity of the Sichuan Basin helped to initiate a steep topographic gradient [e.g., *Clark and Royden*, 2000] that in turn enhances fluvial erosion, further

localizing mass flux and differential rock uplift [e.g., *Willett*, 1999].

9. Conclusions

[67] Analysis of stream profiles along the eastern margin of the Tibetan Plateau adjacent to and north of the Sichuan Basin reveals a systematic geographic distribution of channel steepness. Highest steepness indices (CSI) are spatially associated with the topographic margin of the plateau and occur in a zone ~50–60 km wide adjacent to the Sichuan Basin. North of the basin, steep channels are restricted to a 20–30 km wide band along the crest of the Min Shan. Channel profile concavity throughout the region appears to be directly related to this zone of high steepness index. Channels that flow from the plateau into the zone display low concavities that reflect a relative downstream increase in gradient. This steepening appears to be independent of channel drainage area. Channels that have their headwaters in the zone of high gradient display markedly higher concavities that reflect a relatively rapid downstream decrease in gradient. Small tributaries throughout much of the region have concavities within the range expected for channels experiencing uniform rock uplift and erosive power [*Whipple and Tucker*, 1999]. The region of high stream gradients is spatially associated with the highest topography along the plateau margin, reinforcing suggestions that the bedrock channel network sets much of the relief structure of tectonically active landscapes [*Whipple et al.*, 1999].

[68] Throughout the study area we see little systematic correlation of stream gradient with lithologic variations. The effect of resistant lithology appears to be restricted to local increases in gradient associated with particularly massive, unjointed rocks. Likewise, we see no consistent relation between the channel steepness index and drainage area, as might be expected if sediment flux were responsible for the pattern of channel gradients [e.g., *Sklar and Dietrich*, 1998]. Thus regional differences in channel steepness index point to an external control on channel gradient that we interpret as a region of active differential rock uplift along the plateau margin.

[69] The presence of active rock uplift along this margin is remarkable, given the distinct lack of upper crustal shortening between the plateau and the Sichuan basin [*Burchfiel et al.*, 1995; *Chen et al.*, 2000]. The width of the region of steepest channels suggests that differential rock uplift is driven by localized crustal thickening. A general association between active faults and the region of high stream gradients supports this inference. However, the high concavity of channels in the eastern Min Shan seems to indicate the presence of spatial gradients in rock uplift rate that are not directly associated with discrete faults. Distributed differential rock uplift across this region is consistent with preliminary determinations of incision rate from fluvial terraces, and suggests the possibility that rock uplift in this region may be a combined isostatic and dynamic response to flow in the lower crust [e.g., *Royden et al.*, 1997].

[70] **Acknowledgments.** This research was conducted with support from the Continental Dynamics program at NSF (EAR-9614970 and EAR-9725723). Insightful reviews by Jerome Lavé, Wayne Thatcher, and an anonymous reviewer helped clarify aspects of the manuscript. Discussions with Simon Brocklehurst, Clark Burchfiel, Marin Clark, Kip Hodges, Wiki Royden, and Noah Snyder sharpened our thinking on aspects of the paper. EK wishes to acknowledge the NSF Earth Sciences Postdoctoral Fellowship program and D. Burbank for support at UCSB during the completion of this manuscript.

References

Avouac, J. P., and P. Tapponnier, Kinematic model of active deformation in central Asia, *Geophys. Res. Lett.*, *20*, 895–898, 1993.

Beaumont, C., P. Fullsack, and J. Hamilton, Erosional control of active compressional orogens, in *Thrust Tectonics*, edited by K. R. McClay, pp. 1–18, Chapman and Hall, New York, 1992.

Bilham, R., K. Larson, and J. Freymueller, GPS measurements of present-day convergence across the Nepal Himalaya, *Nature*, *386*, 61–63, 1997.

Brocklehurst, S. H., and K. X. Whipple, Glacial erosion and relief production in the eastern Sierra Nevada, California, *Geomorphology*, *42*, 1–24, 2002.

Burchfiel, B. C., Z. Chen, Y. Liu, and L. H. Royden, Tectonics of the Longmen Shan and adjacent regions, *Int. Geol. Rev.*, *37*(8), 661–735, 1995.

Chen, S. F., and C. J. L. Wilson, Emplacement of the Longmen Shan Thrust-Nappe Belt along the eastern margin of the Tibetan Plateau, *J. Struct. Geol.*, *18*(4), 413–430, 1996.

Chen, S., C. J. L. Wilson, Z. Luo, and Q. Deng, The evolution of the western Sichuan foreland basin, southwestern China, *J. SE Asian Earth Sci.*, *10*, 159–168, 1994a.

Chen, S. F., C. J. L. Wilson, Q. D. Deng, X. L. Zhao, and Z. L. Luo, Active faulting and block movement associated with large earthquakes in the Min Shan and Longmen mountains, northeastern Tibetan Plateau, *J. Geophys. Res.*, *99*, 24,025–24,038, 1994b.

Chen, Z., B. C. Burchfiel, Y. Liu, R. W. King, L. H. Royden, W. Tang, E. Wang, J. Zhao, and X. Zhang, GPS measurements from eastern Tibet and their implications for India/Eurasia intracontinental deformation, *J. Geophys. Res.*, *105*, 16,215–16,227, 2000.

Clark, M. K., and L. H. Royden, Topographic ooze: Building the eastern margin of Tibet by lower crustal flow, *Geology*, *28*(8), 703–706, 2000.

Demoulin, A., Testing the tectonic significance of some parameters of longitudinal river profiles: The case of the Ardenne (Belgium, NW Europe), *Geomorphology*, *24*, 189–208, 1998.

Dirks, P., C. J. L. Wilson, S. Chen, Z. Lou, and S. Liu, Tectonic evolution of the NE margin of the Tibetan Plateau: Evidence from the central Longmen Mountains, Sichuan Province, China, *J. SE Asian Earth Sci.*, *9*, 181–192, 1994.

Editoral Board, State Seismological Bureau, Lithospheric dynamics atlas of China, China Cartogr. Publ. House, Beijing, 1989.

Fielding, E. J., B. L. Isacks, M. Barazangi, and C. Duncan, How flat is Tibet?, *Geology*, *22*, 163–167, 1994.

Flint, J. J., Stream gradient as a function of order, magnitude, and discharge, *Water Resour. Res.*, *10*, 969–973, 1974.

Gilchrist, A. R., H. Kooi, and C. Beaumont, Post-Gondwana geomorphic evolution of southwestern Africa: Implications for the controls on landscape development from observations and numerical experiments, *J. Geophys. Res.*, *99*, 12,211–12,228, 1994.

Hack, J. T., Studies of longitudinal stream profiles in Virginia and Maryland, *U.S. Geol. Surv. Prof. Pap.*, *294-B*, 45–97, 1957.

Hack, J. T., Stream profile analysis and stream-gradient index, *J. Res. U.S. Geol. Surv.*, *1*(4), 421–429, 1973.

Hancock, G. S., R. S. Anderson, and K. X. Whipple, Beyond power: Bedrock river incision process and form, in *Rivers Over Rock: Fluvial Processes in Bedrock Channels*, *Geophys. Monogr. Ser.*, vol. 107, edited by K. J. Tinkler and E. E. Wohl, pp. 35–60, AGU, Washington, D. C., 1998.

Howard, A. D., A detachment-limited model of drainage basin evolution, *Water Resour. Res.*, *30*, 2261–2285, 1994.

Howard, A. D., Long profile development of bedrock channels: Interaction of weathering, mass wasting, bed erosion, and sediment transport, in *Rivers Over Rock: Fluvial Processes in Bedrock Channels*, *Geophys. Monogr. Ser.*, vol. 107, edited by K. J. Tinkler and E. E. Wohl, pp. 297–319, AGU, Washington, D. C., 1998.

Howard, A. D., and G. Kerby, Channel changes in badlands, *Geol. Soc. Am. Bull.*, *94*, 739–752, 1983.

Howard, A. D., M. A. Seidl, and W. E. Dietrich, Modeling fluvial erosion on regional to continental scales, *J. Geophys. Res.*, *99*, 13,971–13,986, 1994.

Jackson, M., and R. Bilham, Constraints on Himalayan deformation inferred from vertical velocity fields in Nepal and Tibet, *J. Geophys. Res.*, *99*, 13,897–13,912, 1994.

Jones, L. M., W. Han, E. Hauksson, A. Jin, Y. Zhang, and Z. Luo, Focal mechanisms of the Songpan earthquakes of August 1976 in Sichuan, China, *J. Geophys. Res.*, *89*, 7697–7707, 1984.

King, R. W., F. Shen, B. C. Burchfiel, L. H. Royden, E. Wang, Z. Chen, Y. Liu, X. Zhang, J. Zhao, and Y. Li, Geodetic measurement of crustal motion in southwest China, *Geology*, *25*, 179–182, 1997.

Kirby, E., Structural, thermal and geomorphic evolution of the eastern margin of the Tibetan Plateau, Ph.D. thesis, Mass. Inst. of Technol., Cambridge, 2001.

Kirby, E., and K. Whipple, Quantifying differential rock-uplift rates via stream profile analysis, *Geology*, *29*(5), 415–418, 2001.

Kirby, E., K. X. Whipple, B. C. Burchfiel, W. Tang, G. Berger, Z. Sun, and Z. Chen, Neotectonics of the Min Shan, China: Implications for mechanisms driving Quaternary deformation along the eastern margin of the Tibetan Plateau, *Geol. Soc. Am. Bull.*, *112*, 375–393, 2000.

Kirby, E., P. Reiners, M. Krol, K. Hodges, K. Whipple, K. Farley, W. Tang, and Z. Chen, Late Cenozoic uplift and landscape evolution along the eastern margin of the Tibetan Plateau: Inferences from $^{40}Ar/^{39}Ar$ and (U-Th)/He thermochronology, *Tectonics*, *21*(1), 1001, doi:10.1029/2000TC001246, 2002.

Kooi, H., and C. Beaumont, Escarpment evolution on high-elevation rifted margins: Insights derived from a surface processes model that combines diffusion, advection, and reaction, *J. Geophys. Res.*, *99*, 12,191–12,209, 1994.

Korzoun, V. I., *Atlas of World Water Nalance*, UNESCO Press, Paris, 1977.

Lavé, J., and J. P. Avouac, Active folding of fluvial terraces across the Siwalik Hills, Himalayas of central Nepal, *J. Geophys. Res.*, *105*, 5735–5770, 2000.

Li, J., S. Xie, and M. Kuang, Geomorphic evolution of the Yangtze Gorges and the time of their formation, *Geomorphology*, *41*, 125–135, 2001.

Massong, T. M., and D. R. Montgomery, Influence of sediment supply, lithology, and wood debris on the distribution of bedrock and alluvial channels, *Geol. Soc. Am. Bull.*, *112*, 591–599, 2000.

Miller, J. R., The influence of bedrock geology on knickpoint development and channel-bed degradation along downcutting streams in south-central Indiana, *J. Geol.*, *99*, 591–605, 1991.

Ministry of Geology and Mineral Resources, *Regional Geology of Sichuan Province*, *Geological Memoirs*, 728 pp., Geol. Publ. House, Beijing, 1991.

Moglen, G. E., and R. L. Bras, The effect of spatial heterogeneities on geomorphic expression in a model of basin evolution, *Water Resour. Res.*, *31*, 2613–2623, 1995.

Molnar, P., and P. England, Late Cenozoic uplift of mountain ranges and global climate change: Chicken or egg?, *Nature*, *346*, 29–34, 1990.

Molnar, P., P. England, and J. Martinod, Mantle dynamics, uplift of the Tibetan Plateau, and the Indian monsoon, *Rev. Geophys.*, *31*, 357–396, 1993.

Montgomery, D. R., and J. M. Buffington, Channel-reach morphology in mountain drainage basins, *Geol. Soc. Am. Bull.*, *109*, 596–611, 1997.

Montgomery, D. R., and E. Foufoula-Georgiou, Channel network source representation using digital elevation models, *Water Resour. Res.*, *29*, 1178–1191, 1993.

Roe, G. H., D. R. Montgomery, and B. Hallet, Effects of orographic precipitation variations on the concavity of steady-state river profiles, *Geology*, *30*, 143–146, 2002.

Royden, L. H., B. C. Burchfiel, R. W. King, Z. Chen, F. Shen, and Y. Liu, Surface deformation and lower crustal flow in eastern Tibet, *Science*, *276*, 788–790, 1997.

Royden, L. H., M. K. Clark, and K. X. Whipple, Evolution of river elevation profiles by bedrock incision: Analytical solutions for transient river profiles related to changing uplift and precipitation rates, *Eos Trans. AGU*, *82*(48), Abstract T62F-09, 2000.

Seeber, L., and V. Gornitz, River profiles along the Himalayan Arc as indicators of active tectonics, *Tectonophysics*, *92*, 335–367, 1983.

Seidl, M. A., and W. E. Dietrich, The problem of channel erosion into bedrock, *Catena Suppl.*, *23*, 101–124, 1992.

Seidl, M. A., J. K. Weissel, and L. F. Pratson, The kinematics and pattern of escarpment retreat across the rifted continental margin of SE Australia, *Basin Res.*, *12*, 301–316, 1996.

Sklar, L., and W. E. Dietrich, River longitudinal profiles and bedrock incision models: Stream power and the influence of sediment supply, in *Rivers Over Rock: Fluvial Processes in Bedrock Channels*, *Geophys. Monogr. Ser.*, vol. *107*, edited by K. J. Tinkler and E. E. Wohl, pp. 237–260, AGU, Washington, D. C., 1998.

Sklar, L., and W. E. Dietrich, Relating rates of fluvial bedrock erosion to rock strength: An experimental study, *Eos Trans. AGU*, *80*(46), Fall Meet. Suppl., F448, 1999.

Sklar, L. S., and W. E. Dietrich, Sediment and rock strength control on river incision into bedrock, *Geology*, *29*, 1087–1090, 2001.

Slingerland, R., S. D. Willet, and H. L. Hennessey, A new fluvial bedrock erosion model based on the work-energy principle, *Eos Trans. AGU*, *78*(46), Fall Meet. Suppl., F299, 1997.

Snyder, N. P., K. X. Whipple, G. E. Tucker, and D. J. Merritts, Evidence for an equilibrium between main-trunk channel incision and tectonic uplift: Mendocino Triple Junction region, northern California, *Geol. Soc. Am. Abstr. Programs*, *31*, A444, 1999.

Snyder, N. P., K. X. Whipple, G. E. Tucker, and D. J. Merritts, Landscape response to tectonic forcing: Digital elevation model analysis of stream profiles in the Mendocino Triple Junction region, northern California, *Geol. Soc. Am. Bull.*, *112*, 1250–1263, 2000.

Stock, J. D., and D. R. Montgomery, Geologic constraints on bedrock river incision using the stream power law, *J. Geophys. Res.*, *104*, 4983–4993, 1999.

Tarboton, D. G., R. L. Bras, and I. Rodriguez-Iturbe, Scaling and elevation in river networks, *Water Resour. Res.*, *25*, 2037–2051, 1989.

Tinkler, K. J., and E. E. Wohl, *Rivers Over Rock: Fluvial Processes in Bedrock Channels*, *Geophys. Monogr. Ser.*, vol. 107, 323 pp., AGU, Washington, D. C., 1998.

Tucker, G. E., and R. L. Slingerland, Erosional dynamics, flexural isostacy, and long-lived escarpments: A numerical modeling study, *J. Geophys. Res.*, *99*, 12,229–12,243, 1994.

Tucker, G. E., and R. Slingerland, Predicting sediment flux from fold and thrust belts, *Basin Res.*, *8*, 329–349, 1996.

Tucker, G. E., and K. X. Whipple, Topographic outcomes predicted by stream erosion models: Sensitivity analysis and intermodel comparison, *J. Geophys. Res.*, *107*(B9), 2179, doi:10.1029/2001JB000162, 2002.

Weissel, J. K., and M. A. Seidl, Inland propagation of erosional escarpments and river profile evolution across the southeast Australian passive continental margin, in *Rivers Over Rock: Fluvial Processes in Bedrock Channels*, *Geophys. Monogr. Ser.*, vol. 107, edited by K. J. Tinkler and E. E. Wohl, AGU, Washington, D. C., 1998.

Whipple, K. X., and G. E. Tucker, Dynamics of the stream-power river incision model: Implications for height limits of mountain ranges, landscape response timescales, and research needs, *J. Geophys. Res.*, *104*, 17,661–17,674, 1999.

Whipple, K. X., and G. E. Tucker, Implications of sediment-flux-dependent river incision models for landscape evolution, *J. Geophys. Res.*, *107*(B2), 2039, doi:10.1029/2000JB000044, 2002.

Whipple, K. X., E. Kirby, and S. H. Brocklehurst, Geomorphic limits to climate-induced increases in topographic relief, *Nature*, *401*, 39–43, 1999.

Whipple, K. X., G. S. Hancock, and R. S. Anderson, River incision into bedrock: Mechanics and relative efficacy of plucking, abrasion, and cavitation, *Geol. Soc. Am. Bull.*, *112*, 490–503, 2000a.

Whipple, K. X., N. P. Snyder, and K. Dollenmayer, Rates and processes of bedrock incision by the Upper Ukak River since the 1912 Novarupta ash flow in the Valley of Ten Thousand Smokes, Alaska, *Geology*, *28*, 835–838, 2000b.

Willett, S. D., Orogeny and orography: The effects of erosion on the structure of mountain belts, *J. Geophys. Res.*, *104*, 28,957–28,981, 1999.

Willgoose, G., A physical explanation for an observed-slope-elevation relationship for catchments with declining relief, *Water Resour. Res.*, *30*, 151–159, 1994.

Wohl, E. E., Bedrock channel morphology in relation to erosional processes, in *Rivers Over Rock: Fluvial Processes in Bedrock Channels*, *Geophys. Monogr. Ser.*, vol. 107, edited by K. J. Tinkler and E. E. Wohl, American Geophysical Union, Washington, D. C., 1998.

Zhao, C., R. Xu, and S. Wang, The special long reversed river section in the Yangtze River reaches, *Geol. Miner. Resour. S. China*, *3*, 33–38, 1997.

Z. Chen and W. Tang, Chengdu Institute of Geology and Mineral Resources, 82 North-3 Section, First Ring Road, Chengdu, Sichuan, China. (cdtwenqing@cgs.gov.cn; zhilchen@mail.sc.cninfo.net)

E. Kirby, Department of Geosciences, Pennsylvania State University, University Park, Pennsylvania, 16802, USA. (ekirby@geosc.psu.edu)

K. X. Whipple, Department of Earth, Atmospheric, and Planetary Sciences, Massachusetts Institute of Technology, Cambridge, MA 02139, USA. (kxw@mit.edu)